

## Headline Articles

## Chemical Consequences of Arylnitrenes in the Crystalline Environment

Akito Sasaki, Loïc Mahé, Akira Izuoka, and Tadashi Sugawara\*

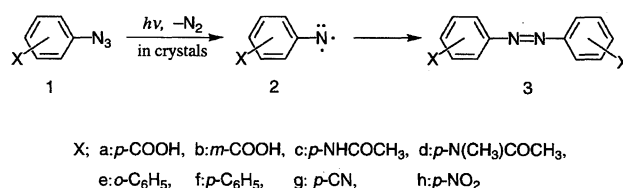
Department of Basic Science, Graduate School of Arts & Sciences, The University of Tokyo,  
Komaba, Meguro, Tokyo 153

(Received December 25, 1997)

UV photolysis of powdered crystals of several aryl azides at cryogenic temperatures afforded azo compounds predominantly. In the cases of *p*-(*N*-methylacetamido)phenyl azide and 2-azidobiphenyl, a CH insertion product or a carbazole was formed, competing with azo formation. These products can be considered to be formed through topotactic processes when the crystal structures are taken into account. The aryl nitrenes generated in the azide crystals were monitored by ESR spectroscopy; they turned out to have extremely long half life-times, compared with those in the gas phase or in solution. Such high kinetic stabilities are ascribed to the inert environment around the generated nitrenes. The decay process of aryl nitrenes in the initial stage obeyed a pseudo-first order kinetics; activation parameters were evaluated by Arrhenius plots. The activation enthalpies and entropies indicate that the diffusional processes of aryl nitrenes may be the vital factors determining the kinetic stability and the product distribution in the crystalline environment.

Chemical reactions are usually carried out in fluid media, such as in a gas phase or in solution. Since the reactant molecules in fluid phases can diffuse freely and isotropically, the kinetic behaviors, such as frequencies of collision, transition probabilities, etc., can be analyzed statistically as a function of concentrations of substrates and reaction temperatures. On the other hand, diffusional behaviors of reactant molecules in crystals are anisotropic and are severely suppressed due to the tight packing in the three-dimensionally ordered arrangement.<sup>1-3)</sup> Chemical reactivity in the solid phase, therefore, depends on the distance and relative orientation of the reaction sites of the reacting molecules.<sup>4-8)</sup> Such a circumstance sometimes leads to a higher regio- and stereoselectivity in the product formation in the solid phase than those in the fluid phases.<sup>9-12)</sup> It is difficult, however, to apply a statistical kinetic treatment to analyze the solid state reactivity. This may be the reason for the scarcity of examples in which the thermodynamic parameters are discussed in detail.<sup>13-15)</sup>

In order to understand and even to control the chemical reactivity in the solid state, it is crucial to investigate the chemical behavior of reactive intermediates in the chemical transformation in question. Higher stability of reactive intermediates in the solid state compared with that in fluid media is advantageous in this respect.<sup>16–18)</sup> Arylnitrene is selected as an intermediate of which the chemical behavior is to be studied in the solid state. It is well known that the ground state of aryl nitrenes is triplet and that it affords different products depending on its spin multiplicity (Scheme 1).<sup>19–21)</sup> Although



Scheme 1. Generation of aryl nitrenes in crystals and formation of azo compounds.

the first excited singlet state of arylnitrenes had been considered to be of a closed-shell structure,<sup>22,23)</sup> the theoretical reinvestigation of arylnitrene by Borden<sup>24,25)</sup> concluded that the first excited singlet is  $^1A_2$ , with a diradical character. If this interpretation is correct, reaction mechanisms involving the singlet nitrenes have to be re-examined. Moreover, chemical behaviors of arylnitrenes in the solid state can be precisely compared with those in other phases, because reactivities of arylnitrenes have been explored extensively in a gas phase,<sup>25)</sup> in solution,<sup>26–28)</sup> or even in rigid matrices.<sup>29–31)</sup> In a gas phase, singlet phenylnitrene undergoes a valence isomerization to give cyanocyclopentadiene eventually. In rigid matrices, singlet phenylnitrene undergoes a ring expansion to afford 1,2,4,6-azacycloheptatetraene, which is detected by IR spectroscopy.<sup>30)</sup> While singlet arylnitrenes yield 3*H*-azepine derivatives in nucleophilic solvents, such as diethylamine, triplet arylnitrenes give rise to azobenzenes and anilines via a coupling or an abstraction process, respectively.<sup>20,27,28)</sup> Such knowledge is valuable for elucidating the characteristic reactivity of arylnitrenes in the solid state.

This paper describes crystal structures of aryl azides carrying a substituent at the *ortho*- (**1e**), *meta*- (**1b**), or *para*-position (**1a**, **c**, **d**). Since an azido group is charge-polarized, as judged from the formation of 1,3-dipolar cycloaddition products,<sup>33</sup> it may operate as an orientation-controlling site in crystals. A substituent on the phenyl group also collaborates with the azido group for regulating the crystal structure of aryl azide.

Photoproducts from aryl azides were interpreted to be formed from the triplet arylnitrenes. The chemical behaviors of arylnitrenes were monitored directly by electron spin resonance (ESR) spectroscopy. The half life-times were found to be remarkably long, suggesting that arylnitrenes were kinetically stabilized in crystals to a great extent. The decay of arylnitrenes in crystals suggests that the diffusional process is the key to product formation.

## Results

**A. Crystal Structures of Aryl Azides.** Crystal structures of aryl azides (**1a**–**e**) carrying various substituents at the *para*-, *meta*-, or *ortho*-position were elucidated by X-ray crystallography. The characteristics of the crystal structures of several aryl azides are as follows.

***p*-Carboxyphenyl Azide (**1a**).** The molecular structure of **1a** is shown in Fig. 1a. It is to be noted that the azido group composed of three nitrogen atoms is not straight, but slightly bent. The bond distances and angles are almost the same as those of the azido groups of which the structures have been determined.<sup>34</sup> The plane formed by the azido group is twisted from the benzene ring by 4.2°. These structural features are commonly observed in the following four azides **1b**–**e** (Fig. 1a). Molecular structure and charge densities of phenyl azide, calculated using a PM3/RHF method, are shown in Fig. 1b. The charge densities of the azido group of aryl azides (**1a**–**e**) are also calculated, and they are basically the same as those of the parent compound. The geometrical feature is reproduced by calculation and the distinct charge distribution in the azido group is also recognized.

In crystals, the carboxyl group of **1a** forms a hydrogen-bonded dimer (molecules A and B) with an O···O distance

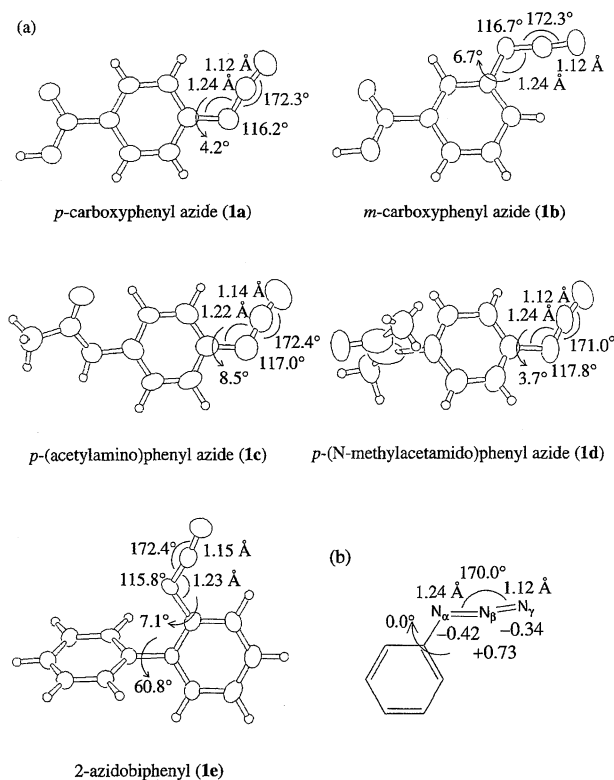


Fig. 1. (a) Molecular structures of aryl azides **1a**–**e**. (b) Calculated charge densities of the nitrogen atoms of azido group.

of 2.62 Å (Fig. 2a). Furthermore, the azido groups of **1a** are *face-to-face* with each other (molecules A and C). As a result, hydrogen-bonded dimers are arranged to form a one-dimensional array along the direction of (2, 0, 2). These arrays are located almost on the same plane, forming a sheet structure. The sheet of azide molecules is stacked nearly along the direction of (−1, 1, 1) with an interplanar distance of 3.42 Å as shown in Fig. 2b. Consequently, a pair of azido groups of **1a** are surrounded by benzene rings of adjacent molecules above and below and at both sides. The intermolecular N<sub>α</sub>···N<sub>α</sub> distance between molecules A and C'' (shown in Fig. 2b) is 4.06 Å, and the N<sub>α</sub>···O distance between molecules A and

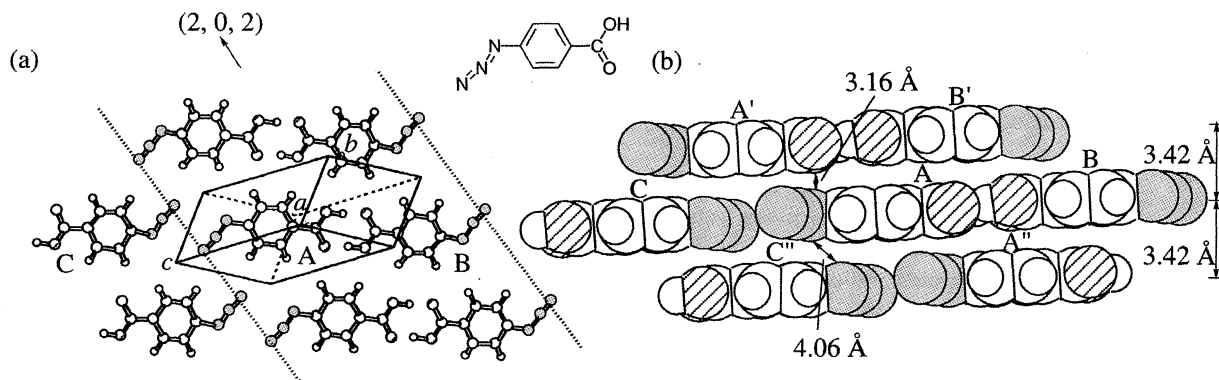


Fig. 2. Crystal structure of *p*-carboxyphenyl azide (**1a**). Triclinic,  $P\bar{1}$ ,  $a = 6.790(2)$ ,  $b = 10.837(3)$ ,  $c = 5.627(3)$  Å,  $\alpha = 94.57(2)$ ,  $\beta = 108.94(2)$ ,  $\gamma = 70.92(2)^\circ$ ,  $Z = 2$ . (a) Hydrogen-bonded dimers of azides **1a** on the same plane, arranged along the direction of (2 0 2). (b) Stacking of azides **1a** along the direction perpendicular to the molecular plane.

A' is as short as 3.16 Å.

***m*-Carboxyphenyl Azide (1b).** The crystal structure of *m*-carboxyphenyl azide **1b** is somewhat similar to that of the *p*-carboxy derivative. As shown in Fig. 3a, azide **1b** also forms a hydrogen-bonded dimer (AB) with an O...O distance of 2.62 Å, and the azido groups face each other (BC). Different from azide **1a**, the hydrogen-bonded dimers are arranged in a zigzag array, which forms a terrace structure stacked along the *c*-axis, as shown in Fig. 3b. The interplanar distance between the terrace-layers is 3.42 Å. In addition, pairs of the facing azido groups of **1b** (B'C', BC, B''C'', etc.) are located *side-by-side*. Consequently, a pair of azido groups form a layered structure along the perpendicular direction (*c*-axis) to the terrace-sheet (Fig. 3b), with a step distance of 1.03 Å. The intermolecular  $N_{\alpha}\cdots N_{\alpha}$  distance between the superimposed azido groups is 3.78 Å.

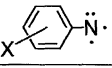
***p*-(Acetylamino)phenyl Azide (1c).** The crystal structure of *p*-(acetylamino)phenyl azide **1c** is very similar to that of acetanilide.<sup>35</sup> A hydrogen-bonded chain (N...O distance 2.85 Å) formed by acetylamino groups is arranged along the *a*-axis (ABCD...). The azidophenyl groups are thus attached like hanging groups of the polymeric hydrogen-bonded chain (Fig. 4a), constructing a corrugated sheet along the *a*-axis. As a result, azido groups belonging to the two adjacent parallel chains on the *ab* plane form a one-dimensional array.

The hydrogen-bonded chains on the *ab* plane are overlapped along the *c*-axis, shifting a half of the repeating unit. Consequently, one-dimensional arrays of azido groups construct a sheet structure, which is perpendicular to the molecular plane as in the case of **1b**, as shown in Fig. 4b. A short intermolecular distance of 3.67 Å is recognized between  $N_{\alpha}$ 's of azido groups along the *c*-axis.

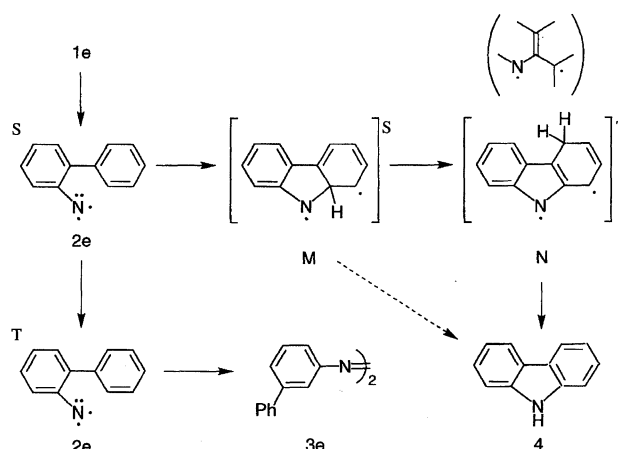
***p*-(*N*-Methylacetamido)phenyl Azide (1d).** The crystal structure of azide **1d** is composed of head-to-head dimers (AB, A'B', etc.) formed by facing azido groups (Fig. 5a). Although hydrogen-bonding substituents are absent in azide **1d**, pairs of azido groups construct a layered structure perpendicular to the *ac* plane, as in the cases of azide **1b** and **1c**. It is to be noted that the azido group of the molecule A' is located close to an *N*-methyl group of the molecule B of the adjacent dimeric pair (A, B), as shown in Fig. 5b. The intermolecular distance between the nitrogen atom ( $N_{\alpha}$ ) of A' and the *N*-methyl group of B is only 3.14 Å, which is much shorter than the distance (3.90 Å) between nitrogen atoms ( $N_{\alpha}$ ) of the facing azido groups (A, B).

**2-Azidobiphenyl (1e).** As shown in Fig. 1e, 2-azidobiphenyl **1e** is not planar, and the molecular structure of **1e** is similar to that of 2-nitrobiphenyl.<sup>36</sup> The dihedral angle between the two phenyl rings is 60.8°. The azide **1e** is arranged *side-by-side* (ABC...) to form a one-dimensional array along the *c*-axis, being aligned to the same orientation (Fig. 6a). The same type of the azide arrays is aligned in parallel on the *ac*-plane, forming a corrugated sheet structure. The orientation of the azide molecules on the above sheet is opposite. As shown in Fig. 6b, the azido groups on the above and below layers face to each other, and they form a columnar stacking along the *c*-axis. This azido column

Table 1. Relative Yields of UV Photolysis of Aryl Azides in Crystals

|  | Products (yield, ±2%) |    |    |       |
|--|-----------------------|----|----|-------|
|  | 3                     | 4  | 5  | 6     |
| <i>p</i> -COOH ( <b>2a</b> )   | > 99                  | —  | —  | —     |
| <i>m</i> -COOH ( <b>2b</b> )   | > 98                  | —  | —  | —     |
| <i>p</i> -NHCOCH <sub>3</sub> ( <b>2c</b> )  | > 98                  | —  | —  | —     |
| <i>p</i> -N(CH <sub>3</sub> )COCH <sub>3</sub> ( <b>2d</b> )                       | 38                    | —  | 59 | Trace |
| <i>o</i> -C <sub>6</sub> H <sub>5</sub> ( <b>2e</b> )                              | 45                    | 44 | —  | —     |
| <i>p</i> -C <sub>6</sub> H <sub>5</sub> ( <b>2f</b> )                              | > 98                  | —  | —  | —     |
| <i>p</i> -CN ( <b>2g</b> )   | > 97                  | —  | —  | —     |
| <i>p</i> -NO <sub>2</sub> ( <b>2h</b> )  | > 97                  | —  | —  | —     |

The UV photolysis was carried out at 77 K and the reaction was terminated at room temperature. 3: Corresponding azo compounds, 4: Carbazole (Scheme 2), 5: Dimeric insertion product, 6: Trimer (Scheme 3).



Scheme 2. Reaction routes in the photolysis of 2-azidobiphenyl (**1e**) in crystals.

is surrounded by the stackings of phenyl groups, as shown in Fig. 6b. The intermolecular  $N_{\alpha}\cdots N_{\alpha}$  distance is 4.77 Å, while the intermolecular  $N_{\alpha}\cdots C_{ortho}$  distance is 3.06 Å.

**B. Product Analyses of the Photochemical Decomposition of Aryl Azides in the Crystalline Environment.** UV irradiation of aryl azides **1a**–**h** in finely ground polycrystalline state was performed for 24 h at 77 K by using an ultra-high pressure mercury lamp with a Pyrex filter and a radiation cut-off filter. Excitation of aryl azides was performed mainly by UV light of 365 nm. The reaction was terminated at room temperature, after a week for **1a** and after 24 h for others; photo-products were then separated by gel permeation chromatography. The product distribution after UV photolysis of aryl azides **1a**–**h** is shown in Table 1.

**a) UV Photolysis of 2-Azidobiphenyl (1e).** It is to be noted that azo compound (**3e**) was formed by UV photolysis of 2-azidobiphenyl **1e** in a comparable amount with that of carbazole (**4**) (Scheme 2). The product ratio of **3e** vs. **4** was drastically different from the product distribution in solution chemistry, and was found to depend on the irradiation temperature: The ratio of **3e**/**4** was 1.0 in the UV irradiation at 123 K, but it decreased to 0.22 in the irradiation at 253 K.

**b) UV Photolysis of *p*-(*N*-Methylacetamido)phenyl**

**Azide (1d).** UV photolysis of azide **1d** afforded an insertion product (**5**) and a small amount of a trimer (**6**), together with azo compound (**3d**) (Scheme 3). The former two products were presumably formed via intermolecular hydrogen abstraction by triplet nitrene, followed by recombination of the resulting biradicals. Azo compound (**3d**) was formed in a considerable amount, as in the case of **1e**. The product ratio of **3d** vs. **5** was found to decrease at higher temperatures of UV irradiation and for shorter irradiation times. The product ratio was 1.6 in the UV irradiation at 123 K for 60 min, and it decreased to 0.11 at 253 K for 2 min (see Ref. 37).

The product distribution of *N*-methyl- $d_3$  derivative (**1d'**) was also examined. The deuterium substitution of the *N*-methyl group, however, did not affect the relative yields of

the photo-products. Namely, the product ratio of **5** vs. **3d** was ca. 3 : 2 regardless of whether the azide compound is **1d** (*N*-methyl- $h_3$ ) or **1d'** (*N*-methyl- $d_3$ ). On the other hand, the decay rate of the aryl nitrenes *N*-methyl- $h_3$  vs. *N*-methyl- $d_3$  exhibited an isotope effect of  $k_H/k_D \approx 2.0$ . Half life-times at 263 K of **2d** ( $h_3$ ) and **2d'** ( $d_3$ ) were 15 and 30 min, respectively.

**c) UV Photolysis of Other Aryl Azides.** Though azides **1d** and **1e** were exceptions, photolysis of other aryl azides (**1a–c**, **1f–h**) was found to afford the corresponding azo compounds (**3a–c**, **3f–h**) exclusively (Scheme 4); the conversion of aryl azides was 10% at most. The substantial retardation of the photodecomposition was observed at the conversion yields higher than 10%. This may be due to the

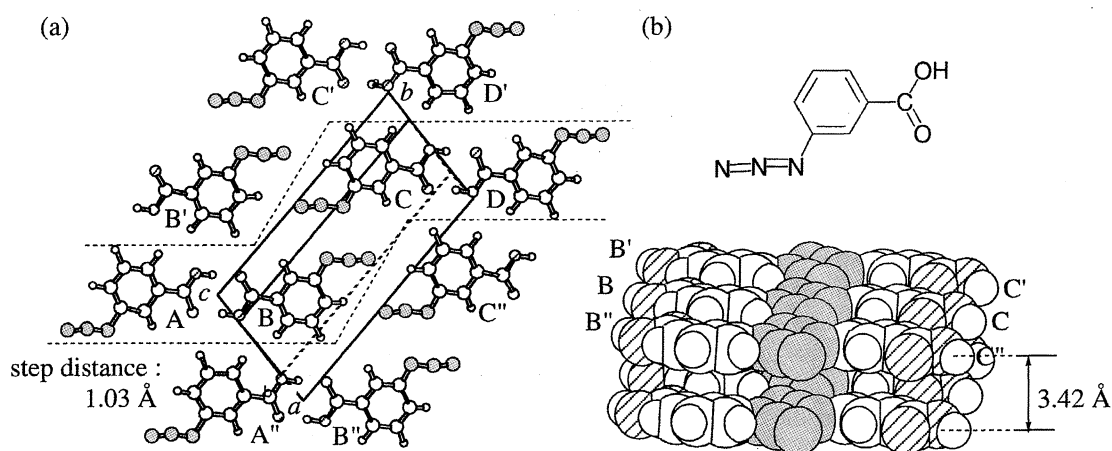


Fig. 3. Crystal structure of *m*-carboxyphenyl azide (**1b**). Triclinic,  $P\bar{1}$ ,  $a = 6.573(1)$ ,  $b = 15.513(3)$ ,  $c = 3.780(1)$  Å,  $\alpha = 94.71(2)$ ,  $\beta = 93.58(2)$ ,  $\gamma = 105.58(2)^\circ$ ,  $Z = 2$ . (a) Terrace-like structure of azide molecules viewed along the  $c$ -axis, (b) Stacking of azide molecules viewed along the  $a$ -axis. The interlayer distance is also shown.

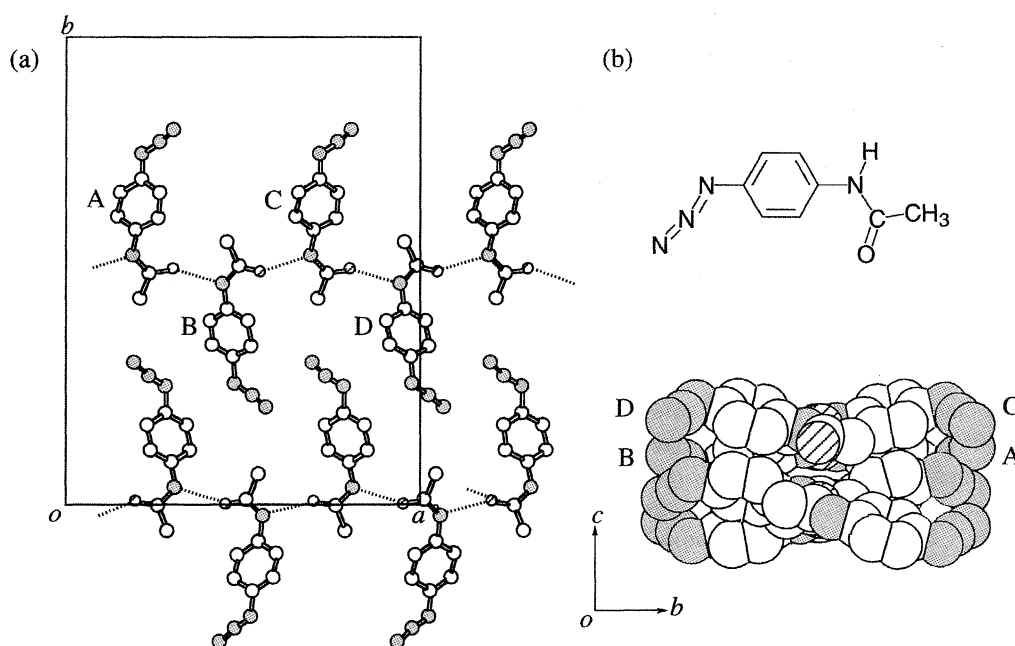


Fig. 4. Crystal structure of *p*-(acetylamino)phenyl azide (**1c**). Orthorhombic,  $Pbca$ ,  $a = 19.322(6)$ ,  $b = 25.398(6)$ ,  $c = 7.311(2)$  Å,  $Z = 16$ . (a) Viewed along the  $c$ -axis, the dotted-lines show hydrogen-bonds ( $N-H \cdots O$ ), (b) viewed along the  $a$ -axis. Hydrogen atoms are omitted.

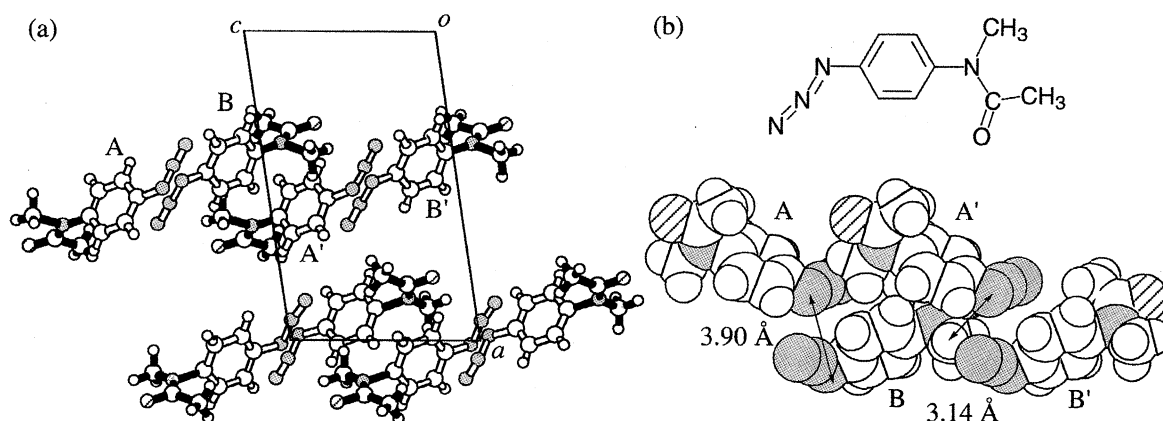


Fig. 5. Crystal structure of *p*-(*N*-methylacetamido)phenyl azide (**1d**). Monoclinic,  $P2_1$ ,  $a = 14.752(3)$ ,  $b = 7.559(1)$ ,  $c = 8.937(2)$  Å,  $\beta = 98.96(2)^\circ$ ,  $Z = 4$ . (a) Viewed along the  $b$ -axis, (b) viewed along the  $a$ -axis.

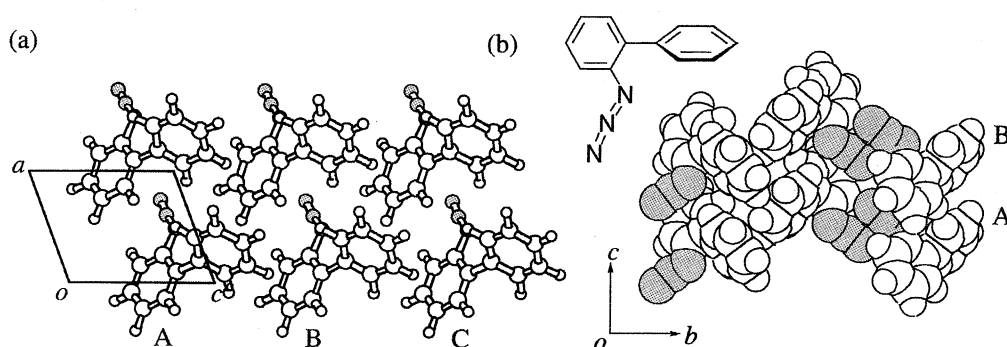
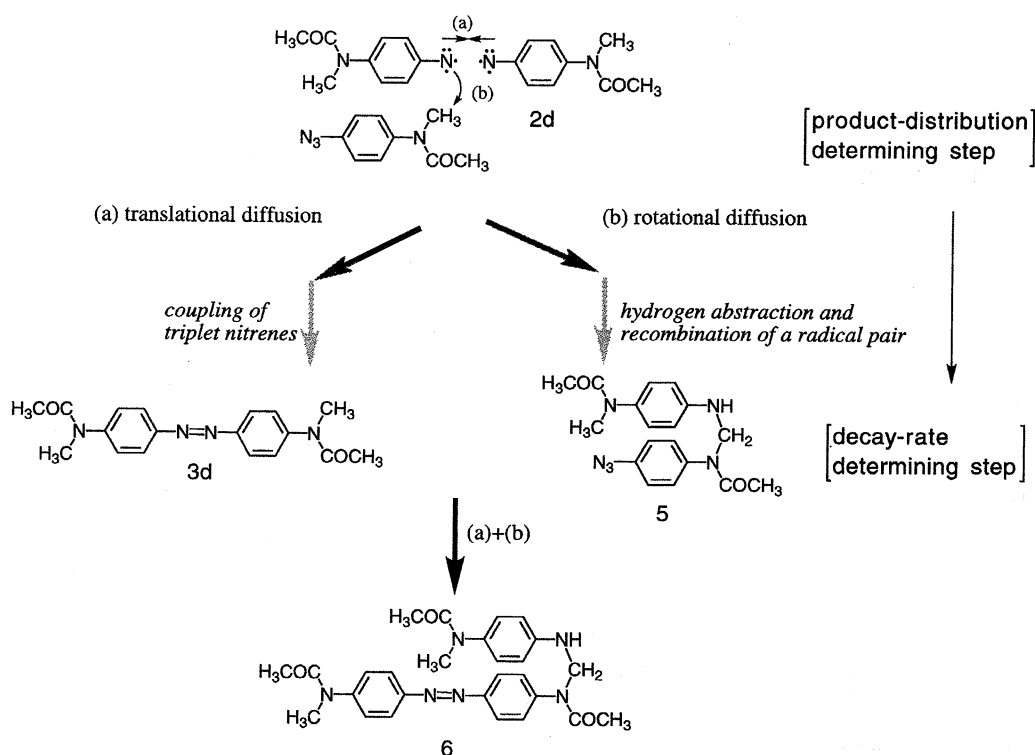
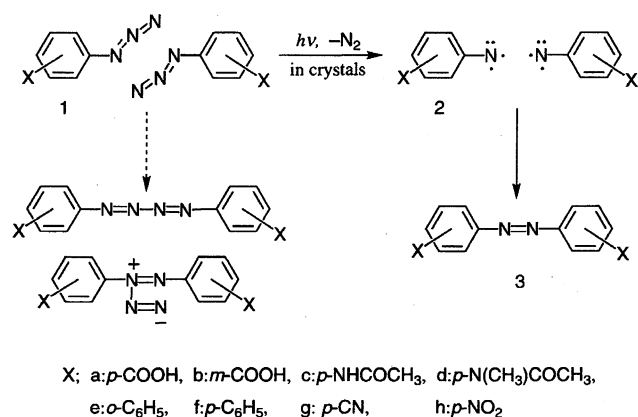


Fig. 6. Crystal structure of 2-azidobiphenyl (**1e**). Monoclinic,  $P2_1/n$ ,  $a = 5.664(3)$ ,  $b = 27.08(2)$ ,  $c = 6.935(4)$  Å,  $\beta = 110.70(4)^\circ$ ,  $Z = 4$ . (a) Viewed along the  $b$ -axis, (b) viewed along the  $a$ -axis.



Scheme 3. Reaction routes in the photolysis of *p*-(*N*-methylacetamido)phenyl azide (**1d**) in crystals.



Scheme 4. Formation of azo compounds.

filtering effect of the resultant arylnitrene.

The chemical transformation of arylnitrene in crystals of *p*-carboxyphenyl azide **1a** was also monitored by IR spectroscopy at 15 K. The peak intensity of the azido group at 2137 cm<sup>-1</sup> was decreased considerably by UV irradiation for 100 min. When temperatures were increased up to 100 K, however, no growth of an absorption peak was detected at all around 1900 cm<sup>-1</sup>. This is the absorption position for the stretching of a cumulative double bond ascribable to 1,2,4,6-azacycloheptatetraene, which is observed, in most cases, in solution or in a rigid matrix as a ring-expanded isomer of the singlet phenylnitrene.

### C. Evolution of Nitrogen Molecules out of the Azide Crystals.

Another photo-product of aryl azides is a nitrogen molecule. After azides were irradiated at 200 K for 30 min, the volume of nitrogen gas which was evolved out of the crystals was analyzed quantitatively as a function of temperatures. Although the change of the gas volume obeyed Boyle–Charles' law up to 250 K, a gradual increase of the gas volume was observed in the cases of *m*-carboxy (**1b**) and *p*-acetylamino (**1c**) derivatives after warming up the samples to temperatures higher than 253 K (Fig. 7a). The increase was accelerated at around 293–313 K, suggesting that the

escape of nitrogen molecules out of the crystals occurs at an appreciable rate. On the other hand, the volume change in the case of **1a** was almost linear even up to 373 K, and then the experimental plot deviated upward, showing a sudden increase of the gas volume at around 403 K (Fig. 7b).

### D. ESR Detection of Arylnitrenes Generated in Host Crystals of Aryl Azides.

**a) Detection of Arylnitrenes Generated in Crystals.** We measured the ESR spectra of arylnitrenes **2a–h** which had been photochemically generated in powdered crystals of azides **1a–h**. In the spectra, a characteristic triplet signal was observed. Resonance peaks at the field around 660 mT were assignable to the *X*, *Y* transitions, and a weak peak observed at around 730 mT was assigned to the *Z* transition (for example, see Fig. 8). Although the *X* and *Y* transitions were overlapped at cryogenic temperatures (*T* < 150 K), they were gradually split with increasing the temperature to beyond 150 K. The zero-field splitting (zfs) parameters  $|D|$ ,  $|E|$  are summarized in Table 2. Hyperfine structures (hfs) with a coupling constant  $a_N$  of 1.9 mT were observed on the *Y* transition of the triplet signal of each arylnitrene.

Photolysis of **1e** afforded not only a triplet signal of **2e** but also another triplet signal ascribable to a biradical at around 300 mT. The zfs parameters ( $|D|$ ,  $|E|$ ) of the latter species are 0.0225 and 0.0010 cm<sup>-1</sup>, respectively (Fig. 8). The triplet spectrum of the biradical also shows hfs with a coupling constant  $a_N$  of 1.3 mT on the *Y* transition.

In the cases of nitrenes **2d** and **2f**, there appeared a small but distinct signal around 240 mT, besides the *X*, *Y* transitions of the triplet nitrene at 660 mT (Fig. 9). The former signal may be assigned to a quintet species (*Q*) derived from the magnetically coupled nitrene pair (vide infra).

### b) Kinetic Stability of Arylnitrenes in the Crystalline Environment.

The decay of the triplet arylnitrenes **2a–h** was monitored by the decrease of the intensity of the *X* transition in the ESR spectra; the nitrenes turned out to demonstrate unusual kinetic stability in crystals. Their half life-times at 300 K are in a range of a few minutes to a few hours. Nitrene

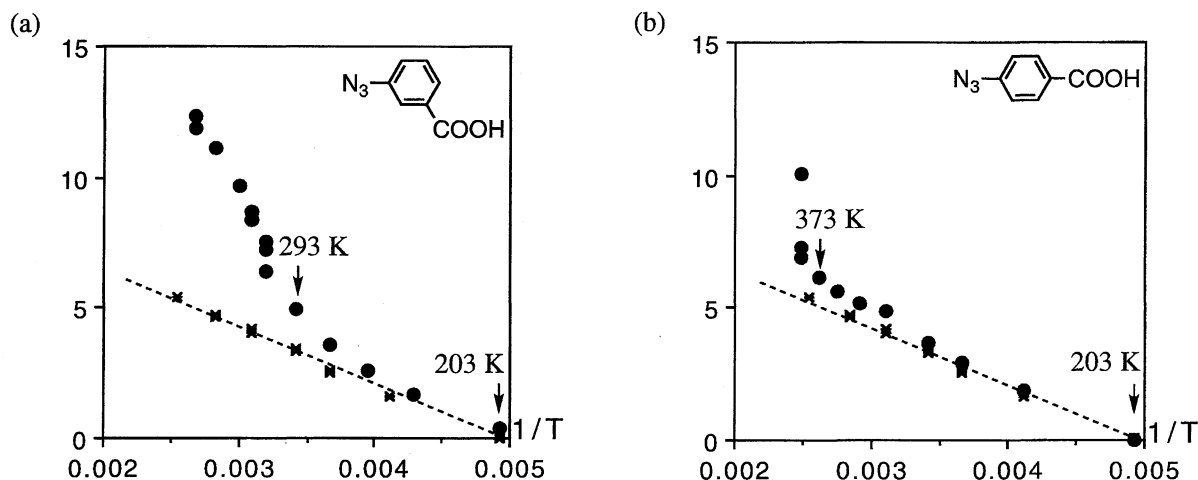


Fig. 7. Volume change caused by extruded nitrogen molecules out of the azide crystals when the crystals were warmed after UV irradiation at 203 K for 30 min. (a) In the case of *p*-carboxyphenyl azide (**1a**), (b) in the case of *m*-carboxyphenyl azide (**1b**). Marks (x) depict the volume change before irradiation.

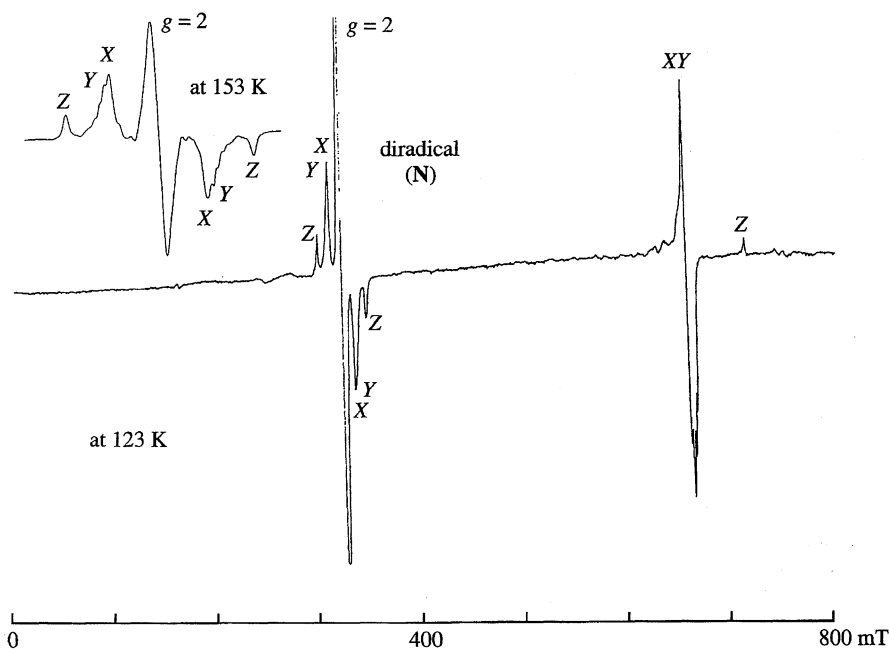
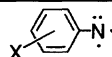


Fig. 8. ESR spectrum of 2-nitrenobiphenyl (**2e**). A triplet signal at the central region was assignable to a diradical (N).

Table 2. Zero-Field Splitting Parameters of Arylnitrenes (**2a–h**) Generated in Crystals at 8 K

|  | $D$ (cm <sup>-1</sup> ) | $E$ (cm <sup>-1</sup> ) |
|---|-------------------------|-------------------------|
| <i>p</i> -COOH ( <b>2a</b> )  | 0.981                   | 0.0006                  |
| <i>m</i> -COOH ( <b>2b</b> )  | 0.975                   | 0.0008                  |
| <i>p</i> -NHCOCH <sub>3</sub> ( <b>2c</b> )   | 0.947                   | 0.0009                  |
| <i>p</i> -N(CH <sub>3</sub> )COCH <sub>3</sub> ( <b>2d</b> )                        | 1.004                   | 0.0008                  |
| <i>o</i> -C <sub>6</sub> H <sub>5</sub> ( <b>2e</b> )                               | 0.994                   | 0.0008                  |
| <i>p</i> -C <sub>6</sub> H <sub>5</sub> ( <b>2f</b> )                               | 0.903                   | 0.0010                  |
| <i>p</i> -CN ( <b>2g</b> )  | 0.959                   | 0.0007                  |
| <i>p</i> -NO <sub>2</sub> ( <b>2h</b> )   | 0.978                   | 0.0015                  |

**2a**, in particular, has an extraordinarily long half life-time of about ten days in crystals (see Table 3 for details).<sup>38)</sup>

**E. Temperature Dependence of the ESR Signals.** The temperature dependence of the intensities of ESR signals of aryl nitrenes was measured in detail for the following three species: a) a triplet nitrene, b) a magnetically coupled pair of triplet diradical derived from nitrene **2e**.

First, temperature dependence of the triplet signal intensity was examined for aryl nitrenes generated photochemically in the mother crystals of aryl azides. The intensity of the X, Y transitions of the triplet signal of the aryl nitrene, e.g. **2a**, around 660 mT turned out not to obey the Curie law. Namely, the Curie plot for the nitrene showed a slight deviation from

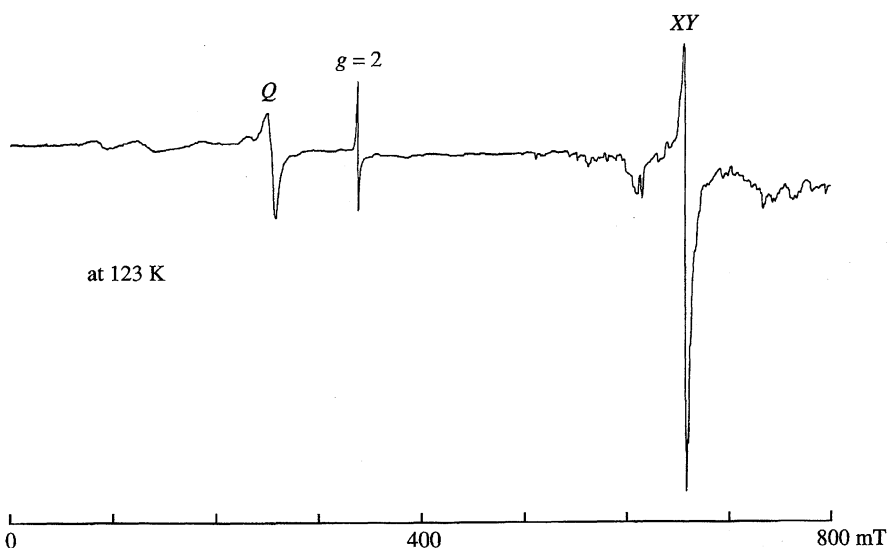
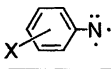


Fig. 9. ESR spectrum of 4-nitrenobiphenyl (**2f**). A signal at 240 mT was assignable to a quintet species derived from the magnetically coupled nitrene pair.

Table 3. Half Life-Times of Arylnitrenes at 300 K, and Activation Parameters of Azo Formation in the Crystalline Environment

|  | Mp<br>°C | Density<br>g cm <sup>-3</sup> | <i>t</i> <sub>1/2</sub> | $\Delta G_{300}^\ddagger$<br>kJ mol <sup>-1</sup> | $\Delta H_{300}^\ddagger$<br>kJ mol <sup>-1</sup> | $\Delta S_{300}^\ddagger$<br>J mol <sup>-1</sup> K <sup>-1</sup> |
|---|----------|-------------------------------|-------------------------|---|---|--|
| <i>p</i> -COOH ( <b>2a</b> )  | 180      | 1.51                          | 10 d                    | 109   | 95  | -44  |
| <i>m</i> -COOH ( <b>2b</b> )  | 165      | 1.47                          | 14 min                  | 90  | 29  | -203   |
| <i>p</i> -NHCOCH <sub>3</sub> ( <b>2c</b> )                                       | 124      | 1.31                          | 64 min                  | 94  | 33  | -205   |
| <i>p</i> -C <sub>6</sub> H <sub>5</sub> ( <b>2f</b> )                             | 83       | 1.35                          | 5 min                   | 87  | 70  | -59  |
| <i>p</i> -CN ( <b>2g</b> )  | 70       | 1.30                          | 11 min                  | 90  | 37  | -177   |
| <i>p</i> -NO <sub>2</sub> ( <b>2h</b> )   | 74       | 1.42                          | 2.5 h                   | 96  | 29  | -197   |

a straight line at lower temperature ( $T \leq 20$  K). Second, a signal ascribable to the quintet dimer of nitrenes was observed at 260 mT, especially in the spectra of **2d** and **2f**. The temperature dependence of the quintet signal intensity exhibits a thermally populated pattern in the case of **2f**. The maximum of the peak intensity was observed around 8 K (Fig. 10). Third, in the spectra of **2e**, the triplet signal which is assignable to the diradical species was observed at 300 mT, as shown in Fig. 8. The signal intensity of the diradical showed a linear temperature dependence in the temperature range of 6–120 K. The signal intensity, however, increased abruptly at 120 K (Fig. 11), whereas the temperature dependence of the nitrene signal does not show any anomaly in this temperature range. The result suggests that the singlet precursor (**M**) of the triplet diradical existed in the photolyzed sample and it started to convert to the triplet species (**N**) at an appreciable rate at temperatures higher than 120 K (see Scheme 2).

The temperature dependence of the line shapes of the triplet ESR signals of nitrenes (**2a–h**) was cautiously ex-

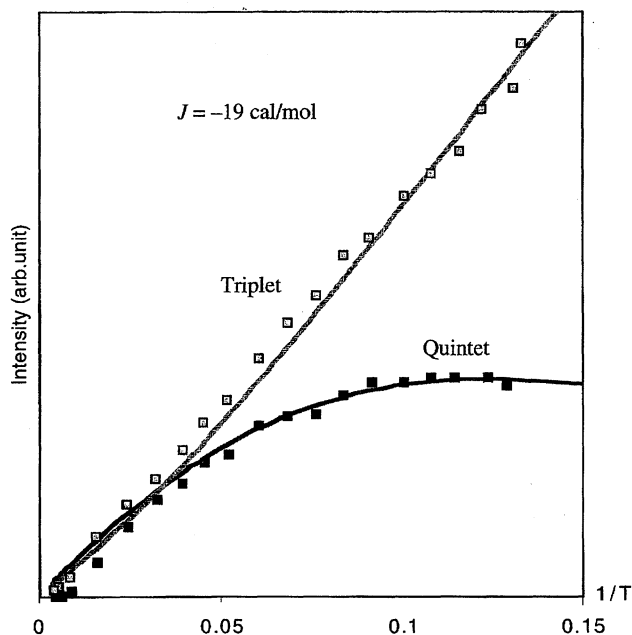


Fig. 10. Temperature dependence of the intensity of triplet and quintet signals in the ESR spectra of 4-nitrenobiphenyl **2f**. The calculated values are also shown by a gray line for the triplet and by a black line for the quintet.

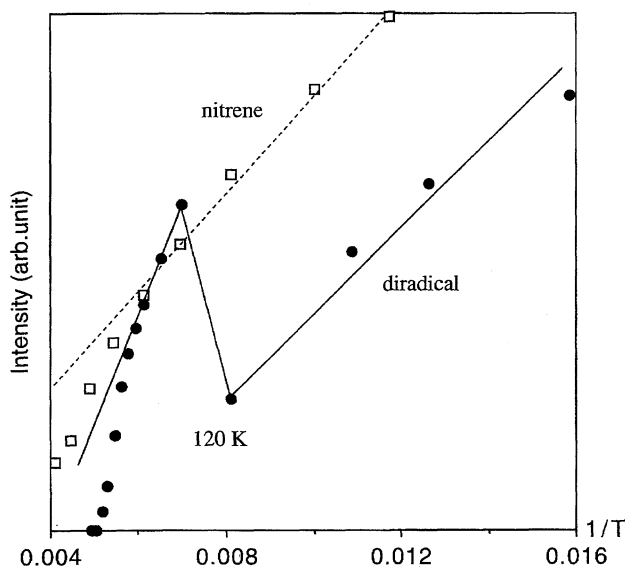


Fig. 11. Temperature dependence of the triplet signal intensity of nitrene **2e** and diradical **N**. The signal intensity of **N** shows abrupt increase at 120 K.

amines. While the  $|D|$  value of the geminate nitrenes **2a–h** decreased slightly with raising the temperature, the temperature dependence of the  $|E|$  value showed the opposite tendency. In the case of nitrene **2a**, in particular, a new triplet signal started to appear around 150 K at the expense of the original signal, which was entirely replaced by the former at 300 K (Fig. 12a). The new species was characterized by new zfs parameters of larger  $|D|$  and smaller  $|E|$  values ( $|D| = 0.969$  cm<sup>-1</sup>,  $|E| = 0.002$  cm<sup>-1</sup> at 243 K) than those of the original ( $|D| = 0.955$  cm<sup>-1</sup>,  $|E| = 0.003$  cm<sup>-1</sup> at 243 K). The irreversible spectral change may be coupled with the structural transformation from the geminate nitrene pair to the relaxed pair (Fig. 12b; also see Discussion).

#### F. Kinetic Analysis of the Decay of the Triplet Nitrene Signal in the Process of Azo Formation.

The chemical decay of aryl nitrenes was monitored by the decrease of the signal intensity of the triplet nitrenes. The decay rates in the initial stage (for 20–30 min) obeyed a pseudo-first order kinetics, but deviated from the straight line gradually. Typical traces are shown in Fig. 13 for **2c** and **2d**. Half life-times ( $t_{1/2}$ ) of the aryl nitrenes in the crystalline environment were evaluated by the following equation:  $t_{1/2} = \ln 2/k$ , where  $k$  is the decay rate in the initial stage (Table 3).



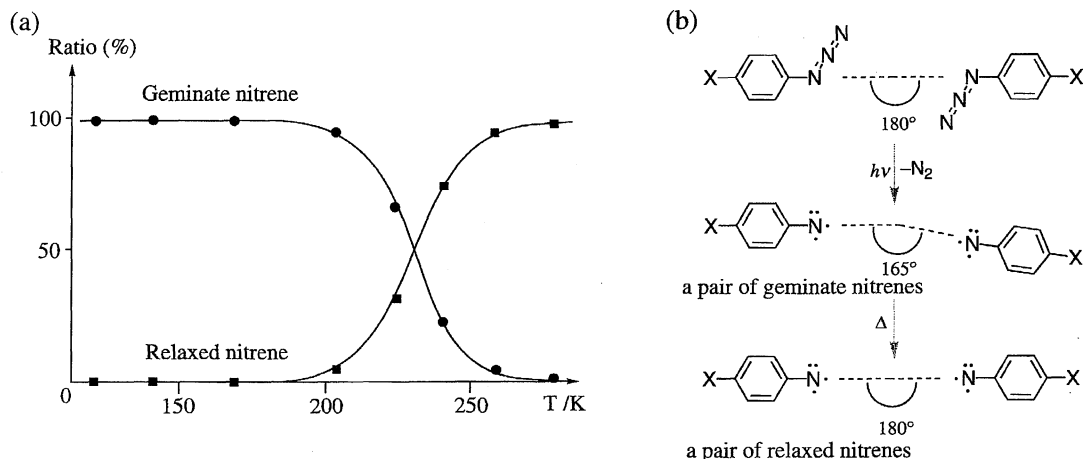


Fig. 12. (a) Relative ratio of a generated nitrene and a relaxed nitrene as a function of temperature. (b) Irreversible geometrical change from a geminate nitrene pair to a relaxed one.

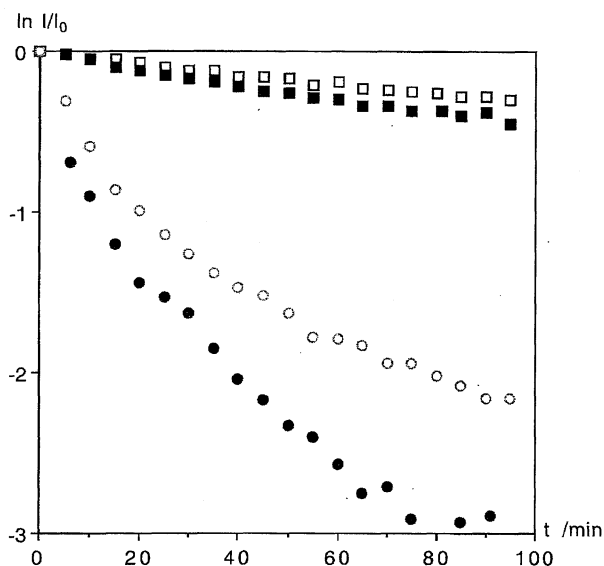


Fig. 13. Chemical decay of nitrenes in crystals *p*-(acetyl-amino)phenylnitrene **2c** at 273 K (□), at 283 K (■), *p*-(*N*-methylacetamido)phenylnitrene **2d** at 263 K (○), at 273 K (●).

Temperature dependence of the decay rates of aryl nitrenes was also examined. The thermodynamic parameters were estimated by the Arrhenius plots of the decay rates of aryl nitrenes at the initial stage in the temperature range of 240–300 K (330–370 K for **2a**). The values of activation enthalpy ( $\Delta H^\ddagger$ ) and entropy ( $\Delta S^\ddagger$ ) of the decay of some nitrenes are listed in Table 3. The activation enthalpies turn out to range from 95 kJ mol<sup>-1</sup> for **2a** to 29 kJ mol<sup>-1</sup> for **2h**. The activation entropies of **2a** and **2f** are -44 or -59 J mol<sup>-1</sup> K<sup>-1</sup>, respectively, while those for the others show very large negative values in a range of -205–160 J mol<sup>-1</sup> K<sup>-1</sup>.

### Discussion

#### A. Reaction Environment Formed by Aryl Azides.

According to the X-ray crystallographic analysis of aryl azides **1a**–**e**, azido groups exhibit a tendency to be arranged,

facing to each other, in an anti-parallel manner. In order to elucidate the origin for this arrangement, the degree of the charge polarization of the azido groups was calculated by a PM3 method. The alpha and gamma nitrogens to the phenyl ring ( $N_\alpha$ ,  $N_\gamma$ ) are -0.4 and -0.3, respectively, and that of the beta nitrogen ( $N_\beta$ ) is +0.7 (Fig. 1b). The electrostatic interaction between the charge polarized azido groups may be the reason for the *face-to-face* and also for the *side-by-side* arrangement of azido groups. Intermolecular distances between nitrogen atoms in the azide pair are summarized in Fig. 14. Some of the distances between nitrogen atoms are comparable with the sum of the van der Waals radius (1.65 Å) of the nitrogen atom. The data suggest that the in-

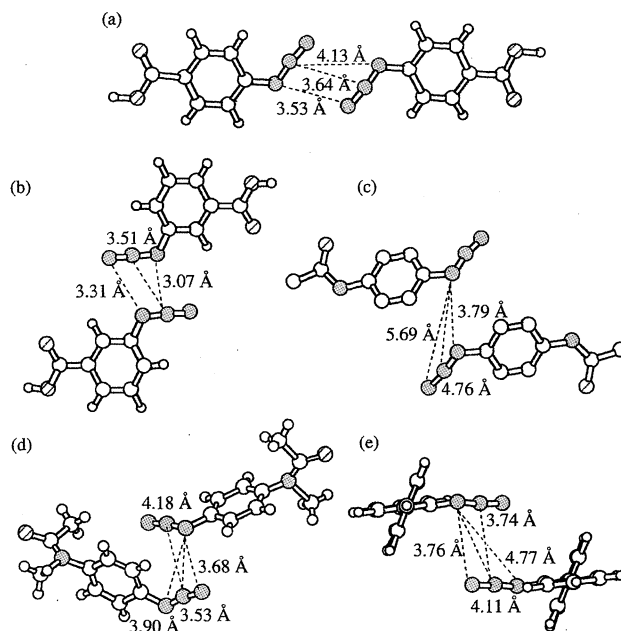


Fig. 14. Intermolecular distances between nitrogen atoms of azido groups (a) *p*-carboxyphenyl azide (**1a**), (b) *m*-carboxyphenyl azide (**1b**), (c) *p*-(acetylamino)phenyl azide (**1c**), (d) *p*-(*N*-methylacetamido)phenyl azide (**1d**), (e) 2-azido-biphenyl (**1e**).

termolecular interaction between the azido groups in rather strong.

Beside the intermolecular interaction between the facing azido groups, a substituent introduced to the phenyl ring also plays a significant role in determining the crystal structure. Azides **1a**–**c**, in particular, bear a hydrogen-bonding substituent, the intermolecular force of which may be more influential than that which operates between the facing azido groups. Azide **1c** is an example of this category; azido groups in the crystal of **1c** are hung to the one-dimensional hydrogen-bonded chain. On the other hand, the intermolecular forces between azido pairs is an influential factor for determining the crystal structures of **1d** and **1e**, which are absent from hydrogen-bonding substituents.

The crystal structures of aryl azides **1a**–**e** are classified into two types in terms of the arrangement of azido pairs. In crystals of *p*-carboxyphenyl azide **1a**, pairs of azido groups are surrounded by benzene rings of the adjacent azide molecules. This stacking is classified as a Type A structure. On the other hand, in crystals of *m*-carboxyphenyl or *p*-(acetylamino)phenyl azide, etc., azido pair are arranged *side-by-side*, forming a layered structure perpendicular to the molecular plane. Such an arrangement is called a Type B structure (Fig. 15).

Aryl azides (**1a**–**d**, **1g**, and **1h**) carry a polar substituent, such as a carboxy, amido, cyano, or nitro group, besides the azido group. Therefore, cancellation of the partial charges of these substituents may be the factor for governing the arrangement of aryl azides. There are two modes of arrangements based on the intermolecular electrostatic interaction: a) anti-parallel stacking of azide molecules with an interaction between the azido group and the polar substituent at both end; b) parallel and slightly shifted stacking of azide molecules with an interaction between the azido groups or between the polar substituent, respectively, at each end. According to the above classification, the crystal structures of *p*-carboxyphenyl azide **1a** is to be classified as Type A, in which azide **1a** stacks in an anti-parallel manner, and the azido group is close to the carboxyl group of the overlapping molecule. On the other hand, the crystal structures of azides

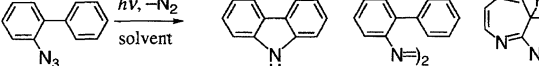
**1b**–**e** are of Type B.

### B. Chemical Consequences of Arylnitrenes in the Crystalline Environment. a) Intramolecular Addition vs. Azo Formation.

As shown in Table 4, the product distribution of 2-azidobiphenyl **1e** in the crystalline environment is found to be different from that in solution. UV photolysis of **1e** in solution affords carbazole selectively, although an insertion product of the nitrene into its own benzene ring is trapped as a 3*H*-azepine derivative in the presence of a secondary amine.<sup>39,40</sup> Thus, it is necessary to use a triplet sensitizer for obtaining an azo compound selectively.<sup>41</sup> Contrastingly, almost equal amounts of an azo compound and carbazole were produced in the solid state reaction of azide **1e** (Scheme 2). The result strongly suggests that the azo compound is more easily produced in the crystalline environment than in solution.<sup>42</sup>

The ESR spectroscopic study reveals that the triplet diradical is also generated independently from **2e**. The abrupt increase of the signal intensity of the triplet diradical at 120 K revealed that the additional triplet diradical was generated thermally when the photolyzed sample was warmed up (Fig. 11). This phenomenon suggests that a singlet precursor for the triplet diradical is present in the photolysate. This precursor may be assigned to the singlet diradical (**M**) formed by addition of the singlet nitrene of the open-shell structure (<sup>1</sup>A<sub>2</sub>) to the phenyl ring (Scheme 2), and it undergoes hydrogen-migration to afford diradical **N** at higher temperatures.

Table 4. Product Ratio in the Photolysis of 2-Azidobiphenyl in Solution and in Crystals (123 K)

|  |       |      |    |
|--|-------|------|----|
| Benzene  | 71    | 11   |    |
| Diethyl ether  | 74    | 9    |    |
| 2-Propanol   | 68    | 12   |    |
| Diethylamine/THF (95%)   | 49    |      | 33 |
| Acetophenone/benzene   | Trace | > 40 |    |
| in Crystals  | 44    | 45   |    |

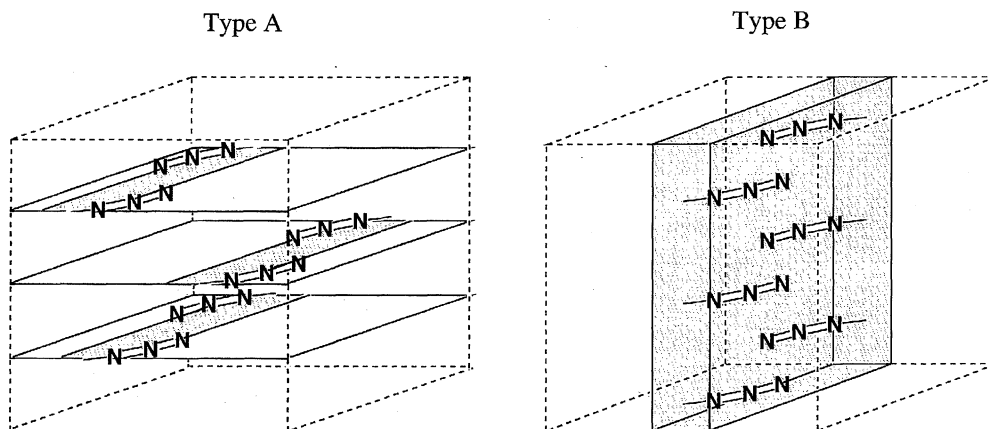


Fig. 15. Classification of crystal structures of aryl azides by arrangement of azido pairs: Type A: one-dimensional array, Type B: layered structure.

Since the diradical **N** can also be expressed by the closed-shell structure, the ground state spin multiplicity of **N** is considered to be singlet. The temperature dependence of the triplet signal of **N**, however, obeyed the Curie law down to 8 K. Consequently, the S–T gap of **N** should be negligibly small. The close resemblance of the zero-field splitting parameter of **N** to that of trimethylenemethane is supporting evidence for the above assignment. Such a reactivity of **2e** is presumably a reflection of the open-shell electronic structure of the singlet nitrene as documented by Borden.<sup>24,25</sup> At elevated temperatures, the diradical **N** affords carbazole eventually through further intra- or intermolecular hydrogen migration(s).<sup>43</sup>

The product ratio **3e/4** turned out to depend on the irradiation temperature (**3e/4** =  $1.0 \pm 0.1$ ,  $0.22 \pm 0.03$  at 123, 253 K, respectively). The phenomenon may be explained as follows. If the irradiation is performed at higher temperatures, the conformational change of the generated singlet nitrene **2e** takes place more easily and adds to the phenyl ring intramolecularly, affording carbazole **4** via the triplet diradical intermediates.

#### b) Intermolecular Abstraction vs. Azo Formation.

The nitrene **2d** generated in the crystal of *p*-(*N*-methylacetamido)phenyl azide **1d** is located not only in front of a nitreno or an azido group of the facing molecule, but also in proximity to an *N*-methyl group of the adjacent azide. Then it is not strange that the insertion product **5** is detected together with azo compound **3d**. When the remaining azido group of inserted product **5** is converted to nitrene, it further reacts with the adjacent nitrene to give rise to azo compound **6**.

Since the activation energy for formation of an azo compound in a fluid medium is estimated to be practically zero<sup>44</sup> and that of hydrogen abstraction by aryl nitrene to be ca. 42 kJ mol<sup>-1</sup>,<sup>45</sup> the difference in activation energies for both processes can hardly explain the obtained product ratio. Therefore, the product distribution observed here is considered to be controlled by the diffusional processes of aryl nitrenes in crystals. Namely, azo compound **3d** is presumably obtained through a translational diffusion and the insertion product **5** is formed through a rotational diffusion.

When the photolysis is carried out at lower temperatures for a prolonged time, the probability of the facing azides being converted to a pair of nitrenes becomes high. If the barrier to the translational diffusion is lower than that of the rotational diffusion (Scheme 3), the generated nitrenes are likely to afford an azo compound preferentially (**3d/5** =  $1.6 \pm 0.1$ ). But if the photolysis is carried out at higher temperatures and the irradiation time is short, the formation of the insertion product is favored (**3d/5** =  $0.11 \pm 0.01$ ). The fact that the product ratio does not reflect the decay rates of the nitrenes **2d** and **2d'** suggests that the product distribution is pre-determined by these diffusional processes, which take place prior to the chemical decay processes. On the other hand, the decay rates may be determined by the barrier of hydrogen/deuterium abstraction after the branching step which is controlled by the diffusional processes.

**c) Exclusive Formation of Azo Compound.** In the Type

B crystals, the generated nitrenes **2b–e** are surrounded by azido or nitreno groups of the surrounding molecules. Thus, the generated nitrenes may react with a nitreno group of the adjacent molecule to yield an azo compound. In the case of azide **1c**, the distance between nitrogen atoms ( $N_\alpha$ ) of the facing azide molecules **1c** is 3.79 Å. The distance of 3.66 Å between nitrogen atoms ( $N_\alpha$ ) of the stacking azide molecules along the *c*-axis is even shorter. Thus, an azo compound may be formed through the diffusional process along this direction.

As will be discussed later, most of the nitrenes are considered to be generated as facing nitrene dimers. There should be, however, a few sites where a nitrene faces an unreacted azido group. It cannot be denied, therefore, that the generated nitrene may react with an azido group of the adjacent molecule to afford an azo compound via 1,2- or 1,4-tetraazabutadiene (Scheme 4). Although these intermediates have been reported in the gas phase experiment,<sup>46–48</sup> they could be produced only when an azido group is attacked by a singlet nitrene. Since the ST energy gap is large, the probability for nitrene to be populated thermally to the singlet state is low. Accordingly, such precursors (1,2- or 1,3-tetraazabutadiene) can be formed rarely, unless the photochemically generated singlet nitrene has enough excess energy to diffuse before being deactivated. In solution, a singlet nitrene is very reactive and undergoes a valence-isomerization much faster than bimolecular reactions.<sup>49–51</sup> IR spectroscopic data for **1a**, however, indicate that the aryl nitrene generated in crystals does not undergo a valence-isomerization. This phenomenon is explained by the lack of space for intramolecular addition to form an azirine intermediate. The generated singlet nitrene immediately undergoes an intersystem-crossing to the ground state triplet nitrene and it stays as it is until the diffusional collapsing occurs with the facing nitrene. This shows a drastic difference from the chemical behaviors of the nitrene generated in a rigid matrix or in solution.

#### C. Reluctance of Nitrogen Molecules to Escape out of the Photolyzed Azide Crystals.

Nitrogen molecules eliminated by UV irradiation of azide crystals turned out to remain inside the crystal even after warming up of the photolyzed crystals. Although escape of nitrogen molecules out of the crystals of *m*-carboxy **1b**, *p*-acetylamino **1c** derivatives starts to occur at temperatures higher than 273 K, the nitrogen molecules extruded from *p*-carboxyphenyl azide **1a**, in particular, sit in the photolyzed crystal even at temperatures higher than 370 K. The large difference in the escaping tendency of nitrogen molecules out of the crystals may be understood when the difference in the crystal structures of azides is taken into account. In Type B crystals of **1b–d**, a columnar structure composed of azide pairs is recognized, whereas in Type A crystal of *p*-carboxyphenyl azide **1a**, the azide pair is constrained by benzene rings of the adjacent azide molecules above, below and at both sides. However, the channel for nitrogen molecules to escape may be blocked by unphotolyzed azide molecules or by azo compounds which were formed by coupling of facing nitrenes, especially at the surface of the crystal. This phenomenon shows a sharp contrast with the

facile escape of solvent molecules, such as water or alcohols, from inclusion-type crystals.

**D. Factors Influencing the High Kinetic Stability of Arylnitrenes.** The kinetic stability of aryl nitrenes turned out to be extremely high in the crystalline environment. Since there is no correlation between the stability of aryl nitrenes and the macroscopic properties of crystals, such as crystal density or melting point, the reason should be looked for at the molecular level.

The lengths of half life-times of aryl nitrenes **2a—h** (Table 3) can be divided into two groups. One group consists solely of *p*-carboxyphenyl nitrene **2a**, which exhibits an extraordinarily long life-time, and the other consists of the rest **2b—h**, which are much less stable than nitrene **2a**. The particularly high kinetic stability of nitrene **2a** in crystals can be rationalized in terms of the packing pattern of the host crystal of **1a**, belonging to Type A. Namely, the hydrogen-bonded dimers of **1a** are closely stacked in layers, and a pair of azido groups are surrounded by benzene rings of the adjacent molecules above and below and at both sides. The generated nitrenes, therefore, are assumed to be placed in an extremely inert environment. Moreover, the distance between the univalent nitrogen of molecule A and the oxygen of the carboxyl group of molecule A'' (shown in Fig. 2b) is as short as 3.16 Å, suggesting significant electronic interaction between these two sites; the N...O distance is shorter than the sum of the van der Waals radius of nitrogen (1.65 Å) and oxygen (1.60 Å). The extruded nitrogen molecules in Type A crystals are seldom released out of the crystals, and sit in a cage even after gentle annealing up to about 400 K. Therefore, the extruded nitrogen molecules, probably trapped between two facing nitrenes in crystals, may interfere with the coupling reaction of triplet nitrenes in crystals, until flexibility in the crystalline packing increases with raising temperature. This is considered to be an additional reason for the unusual stability of **2a**.

On the other hand, the crystal structures of other aryl azides **1b—e** belong to Type B, where pairs of facing azido groups form a two-dimensional layer perpendicular to the molecular planes. Since the generated nitrenes **2b—e** in crystals of **1b—e** are surrounded only by azido or nitreno groups of the adjacent molecules, the chances for geminate nitrenes to couple to give an azo compound should be higher. In addition, we considered that the extruded nitrogen molecules in crystals are released gradually out of the crystals above room temperature, judging from the result of the quantitative analysis of escaped gas volume. Therefore, nitrenes **2b—e** generated in Type B crystals are less stable than nitrene **2a**.

**E. Generation of Nitrene Pairs by the Photolysis of Aryl Azides.** a) **ESR Spectroscopic Evidence for the Existence of Nitrene Pairs in Crystals.** Arylnitrenes,

generated by UV irradiation of powdered crystals of the corresponding aryl azides at cryogenic temperatures, gave the characteristic triplet signals at ca. 660 mT in the ESR spectra. The position of the signal is almost the same as that obtained for the isolated nitrene in a rigid matrix.<sup>52,53</sup> The temperature dependence of the signal intensity of nitrene **2a**, however,

does not follow the Curie law, but deviates from the straight line. Furthermore, the signals at 240 mT are observed in the spectra of **2d** and **2g**.<sup>54,55</sup> The resonance can be assigned to the quintet species with zfs parameters of  $|D| = 0.328 \text{ cm}^{-1}$  and  $|E| = 0.0003 \text{ cm}^{-1}$  by a third-order perturbational calculation under a high-field approximation. These results indicate that the triplet signal cannot be ascribed to the isolated nitrenes in the ground state. Moreover, according to cautious observation of the temperature-dependent ESR spectra, the triplet signals of nitrenes **2a—h** were found to change irreversibly to the new signals with slightly different zero-field parameters. Such a drastic change in the signals is difficult to explain by an intrinsic structural transformation of the isolated nitrene.

These results may be reasonably interpreted by the presence of a pair of nitrenes which interact magnetically.<sup>56</sup> In other words, the triplet signal in the spectra should be ascribed to the excited triplet state arising from the interaction between two adjacent (facing, for example) nitrenes. The degree of antiferromagnetic interaction in **2g** can be estimated from a simulation curve of the Curie-plots for thermally populated triplet and quintet signals. The experimental plots for both signals were reproduced by  $J = -79 \text{ J mol}^{-1}$  (Fig. 10, see Appendix II, Fig. 17). The coincidence of the estimated  $J$  value strongly suggests that the observed triplet and quintet signals can be ascribed to the same nitrene pair. In the case of *p*-carboxyphenyl nitrene **2a**, the relative orientation of two facing aryl nitrenes is defined by angle  $\theta$ , as shown in Fig. 12b (see Appendix I).

Irreversible change of the triplet signal of **2a** may be ascribed to the change in the relative orientation of nitrenes in the dimeric pair (Fig. 12b). According to the ESR spectrum simulation, the angle between the main axes of each nitrene may be estimated to be  $165^\circ$  for the geminate nitrene. After the temperature is raised, the geminate nitrenes are converted to the relaxed nitrene dimer; the angle between the main axes of the dimer is estimated to be  $180^\circ$ . The relaxing process turns out to be irreversible, so the relaxed geometry of the dimers is maintained when the temperatures of the samples are decreased again. A structural relaxation is considered to occur in order to release the stress<sup>57</sup> accumulated by the photochemical extrusion of nitrogen molecules within the azide pairs. Namely, a pair of nitrenes generated in host crystals of aryl azides is not in a thermodynamically stable geometry. Such a discrete structural change can occur only in a fairly rigid cage formed by the crystal **1a** belonging to Type A structure.

**b) Why Are Nitrene Pairs Generated Efficiently in the Crystalline Environment?**

According to the results described above, a pair of nitrenes is proposed to be generated in a crystalline environment in high efficiency.<sup>58</sup> Such a phenomenon is hard to observe in glassy matrices or in solution. One of the possible interpretations for the predominant generation of dimeric pairs of nitrenes in crystals is as follows. Arylnitrenes generated in crystals turn out to have a very long life-time. Therefore, when one of the azido groups in the dimeric pair is converted to a nitrene by UV irradiation,

there is a chance for the facing azide to be photolyzed to afford another nitrene by further irradiation. And they stay as a dimeric nitrene pair, not collapsing into an azo compound or other products in the crystalline environment. As a result, the probability of finding a pair of nitrenes becomes higher in the prolonged irradiation. If this is the case, one should notice an induction time for appearance of a quintet signal due to the magnetically coupled nitrene pair upon UV irradiation. However no induction time was detected for the rise of the quintet signal. The result conflicts with the above mechanism.

Another possibility is that an induced-decomposition takes place by the side of the photochemically excited azide molecules. The excess energy, which is preserved after extruding a nitrogen molecule, may be transferred to the neighboring azide molecules. If enough energy is accumulated in the vibrational mode of the azido group, the induced-decomposition might take place to afford a second nitrene.<sup>59–61</sup> The mechanism of energy transfer may be considered to proceed as discussed in the cited literature.

**F. Diffusion Control of Product Formation Derived from the Arylnitrenes.** In the case of azide **1d**, in particular, the isotope effect on the product ratio is not consistent with that on the decay rate of nitrene **2d**. The discrepancy may be rationalized by the presence of a diffusional process prior to the decay process. Formation of the products is then considered to be determined by the diffusional processes of the nitrene molecules in crystals (Scheme 3).

In order to understand the chemical reactivity of aryl-nitrenes **2a–c** more precisely, the decay rates of nitrenes **2a–c** generated in crystals were measured and the activation parameters were evaluated based on the temperature dependence of the decay rates. While most of aryl-nitrenes examined afford an azo compound almost exclusively, nitrenes **1d** and **1e** produce the abstraction product (**5**) or the addition product (**4**), besides azo compounds (**3d**, **3e**). Since the contribution of other reaction routes than azo formation to the activation parameters cannot be disregarded in the latter two cases, these experimental data were eliminated from the detailed discussion.

The estimated activation parameters turned out to be scattered over a wide range. Considering that these aryl-nitrenes commonly exhibit a topochemical reactivity to afford azo compounds, one could hardly ascribe the wide variation of the activation enthalpy and entropy to those of coupling reactions of the triplet nitrenes.

Since an azo compound is formed by coupling of the facing triplet aryl-nitrenes, the activation energy is practically zero and should not vary significantly, regardless of the substituent of the phenyl ring. The wide variation in  $\Delta H^\ddagger$ ,  $\Delta S^\ddagger$ , therefore, suggests that the diffusional process, which takes place prior to the chemical reaction along the reaction coordinate, is the rate-determining step in the crystalline environment (Fig. 16). As described above, azide molecules in the Type A crystal of **1a** are strongly combined through a dimeric hydrogen bond between carboxyl groups, and the dimers are tightly packed by hydrogen-bonded dimers above, below and

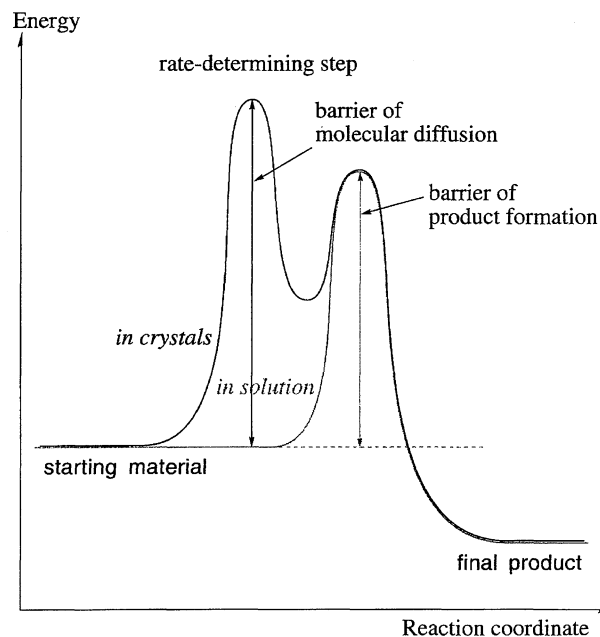


Fig. 16. Difference in the reaction paths between in solution and in crystals.

at both sides. Therefore, the energy barrier of the molecular diffusion in crystals of **1a** is presumed to be very high. At the same time, the relative orientation of the facing nitrenes may be kept almost the same during the chemical transformation in crystals. The situation rationalizes the small activation entropy observed for **2a**, while the small activation enthalpy and the extremely large negative entropy for **2b–g** may reflect a relatively loose packing of **1b–g** in crystals. Since azide molecules **1b–h** may librate in crystals, the diffusional process involves not only the reacting pair but also the surrounding azide molecules in the transition state. The tendency, thus, can also be rationalized when the difference in crystal structures of aryl azides was taken into account.

### Conclusion

Close examination of crystal structures of aryl azides revealed that azido groups play a major role in self-assembling aryl azides based on the electrostatic interaction. The crystal arrangement is thus considered to be an efficient reaction field to form azo compounds, due to the *face-to-face* orientation of azido groups. If such an orientation is realized also in the crystals of di- or triazidobenzene derivatives, oligomeric azo compounds of intriguing substitution patterns may be obtained.

A characteristic feature of the solid state reaction is a high kinetic stability of reactive intermediates involved in the chemical transformation. Arylnitrenes in the crystalline environment, in particular, turned out to exhibit an extraordinary high kinetic stability. Thus one can trace the chemical consequences of reactive intermediates as stable reactant molecules. Detection of the triplet diradical (**M**), which is an intermediate for the formation of carbazole, may be good piece of supporting evidence for the open-shell electronic structure ( $^1A_2$ ) of the first excited singlet state of the aryl-

nitrene. For a diradical intermediate should not be formed if carbazole is formed by a direct insertion of the singlet nitrene to the C–H bond of the intramolecular benzene ring. As shown by the above example, a mother crystal is an excellent matrix for investigating highly reactive intermediates generated photochemically in the crystal. The methodology may be generally applicable to elucidation of the reaction mechanism.

The thermodynamic parameters of the chemical decay of aryl nitrenes evaluated here are informative to understand the chemical behaviors of reactive intermediates in the crystalline environment. Since the parameters reflect the barriers to diffusional process, the product distribution in the solid state is governed not by the activation energy of the chemical reaction but by the barrier to diffusion for aryl nitrene to access one of the reaction sites of the neighboring molecule. This is clear evidence for the concept that the anisotropic diffusional process is crucial to control the product distribution, which is different from that in fluid phases.

On the other hand, the efficient formation of nitrene pairs in the photolyses of azide crystals is rather puzzling. The possibility of induced-decomposition due to energy transfer for the photoexcited azide to the adjacent molecule is of interest from the aspect of a coupling of energy transfer and a bond-cleavage of the weak chemical bond. The detailed mechanisms should be explored in the future.

### Experimental Details

**Preparation of Aryl Azides.** *p*-(*N*-Methylacetamido)phenyl Azide (**1d**). A suspension of *p*-amino-*N*-methylacetanilide (1.73 g, 10 mmol) in  $3.0 \times 10^{-2} \text{ dm}^3$  of 4 M HCl (1 M = 1 mol  $\text{dm}^{-3}$ ) was stirred and then cooled to 0–5 °C. To this suspension was added dropwise a solution of  $\text{NaNO}_2$  (0.77 g, 11 mmol) in  $4.0 \times 10^{-3} \text{ dm}^3$  of  $\text{H}_2\text{O}$ ; the mixture was stirred at 0–5 °C for 1 h. Meanwhile the color of the suspension changed from pink to purple, and finally to yellow. To this solution was added a  $1.2 \times 10^{-2} \text{ dm}^3$  of aqueous solution of  $\text{NaN}_3$  (2.16 g, 30 mmol) with stirring, and then the mixture was allowed to warm up to room temperature, and stirred for an additional hour. The dark-brown oil obtained was extracted with  $\text{CHCl}_3$ , and the extract was dried over anhydrous  $\text{MgSO}_4$ , evaporated, and dried under a reduced pressure. The yield of *p*-(*N*-methylacetamido)phenyl azide was 1.96 g (98%). This crude product was purified by recrystallization from diethyl ether. IR (KBr) 845, 1143 (s, CH), 1304 (vs,  $\text{N}=\text{N}=\text{N}$ ), 1385 (s,  $\text{CH}_3$ ), 1502 (vs, aromatic), 1661 (vs,  $\text{C}=\text{O}$ ), 2099, 2132 (vs,  $\text{N}=\text{N}=\text{N}$ ), 2930  $\text{cm}^{-1}$  (w,  $\text{CH}_3$ );  $^1\text{H}$  NMR (acetone- $d_6$ )  $\delta$  = 1.87 (s, 3H,  $\text{COCH}_3$ ), 3.25 (s, 3H,  $\text{NCH}_3$ ), 7.07 (d, 2H,  $J$  = 8.4 Hz), 7.18 (d, 2H,  $J$  = 8.8 Hz); mp 65 °C.

*p*-(*N*-Methyl- $d_3$ -acetamido)phenyl Azide (**1d'**). A solution of *p*-(acetylamino)phenyl azide (0.85 g, 0.5 mmol) in  $5.0 \times 10^{-3} \text{ dm}^3$  of dry dimethyl sulfoxide was stirred at room temperature, equipped with a drying tube. Sodium hydride (0.85 g, 0.5 mmol) was added to this solution over a period of about ten minutes; immediately hydrogen was generated violently and the colorless solution changed into an orange-red solution. After the mixture was stirred for 10 min, to this solution was added 0.72 g of  $\text{CD}_3\text{I}$  (99.5 atom%D, 0.5 mmol) with stirring, and then the solution became colorless. This solution was poured into excess water, and then the mixture was extracted three times with 10 mL of  $\text{CHCl}_3$ . The extract was

washed with 30 mL of water to remove dimethyl sulfoxide, dried over  $\text{MgSO}_4$ , and concentrated. The crude product was purified by gel permeation chromatography to separate it from the unreacted *p*-(acetylamino)phenyl azide. The yield of *p*-(*N*-methyl- $d_3$ -acetamido)phenyl azide was 0.58 g (63%):  $^1\text{H}$  NMR ( $\text{CDCl}_3$ )  $\delta$  = 1.87 (s, 3H,  $\text{COCH}_3$ ), 7.07 (d, 2H,  $J$  = 8.8 Hz), 7.19 (d, 2H,  $J$  = 8.8 Hz). The deuterium content is estimated to be 99.5 atom%.

**General Procedures for Solid State Photolyses and Product Analyses.** Recrystallized azide samples were finely ground with a mortar and a pestle of agate, and about 150 mg of the polycrystals were placed in a quartz cell (10 × 10 mm). The temperature of the tube was kept at 77 K by immersing the tube into a quartz-windowed liquid-nitrogen Dewar; the samples were irradiated for several hours by an ultrahigh pressure mercury-lamp (Ushio USH-500D), equipped with an Ushio UI-501C mercury lamp set: through a Pyrex filter and a radiation cut-off filter (IRA-25S). After annealing at room temperature, the products were separated by gel permeation chromatography (JAI LC-908). The structures of products were determined by NMR, IR, and mass spectroscopy, as described below. The conversion of the reaction was estimated by measuring the recovered azides.

**Identification of Photoproducts and Determination of Product Distribution.** Azo compounds **3a–h** were identified with those synthesized in an authentic method<sup>63</sup> by means of NMR spectroscopy. Carbazole **4** was identified also by means of NMR. The structure of the insertion products **5** and **6** were determined based on the IR, NMR, and MS spectroscopic data.

**5:** IR (KBr) 838, 1137 (s, CH), 1295 (vs,  $\text{N}=\text{N}=\text{N}$ ), 1386 (s,  $\text{CH}_3$ ), 1506 (vs, aromatic), 1650 (vs,  $\text{C}=\text{O}$ ), 2097, 2129 (vs,  $\text{N}=\text{N}=\text{N}$ ), 2929 (w,  $\text{CH}_3$ ), 3344  $\text{cm}^{-1}$  (s, NH);  $^1\text{H}$  NMR ( $\text{CDCl}_3$ )  $\delta$  = 1.83, 1.85 (s, 3H,  $\text{COCH}_3$ ), 3.21 (s, 3H,  $\text{N}-\text{CH}_3$ ), 4.60 (t, 1H, NH,  $J$  = 7.3 Hz), 5.12 (d, 2H,  $\text{NCH}_2$ ,  $J$  = 7.3 Hz), 6.64 (d, 2H,  $J$  = 8.8 Hz), 6.95 (d, 2H,  $J$  = 8.8 Hz), 7.04 (s, 4H); Mass spectrum  $m/z$  106 ( $\text{CH}_2-\text{NH}-\text{C}_6\text{H}_4$ ), 134 ( $\text{N}(\text{CH}_3)-\text{C}_6\text{H}_4-\text{NHCH}_2$ ), 176 ( $\text{CH}_2-\text{NH}-\text{C}_6\text{H}_4-\text{N}(\text{CH}_3)\text{COCH}_3$ ), 267 ( $\text{CH}_3\text{CON}(\text{CH}_3)-\text{C}_6\text{H}_4-\text{NHCH}_2\text{N}-\text{C}_6\text{H}_4$ ), 352 ( $\text{M}^+$ ).

**6:**  $^1\text{H}$  NMR (Acetone- $d_6$ )  $\delta$  = 1.77, 1.80, 1.83 (s, 3H,  $\text{COCH}_3$ ), 3.00, 3.17 (s, 3H,  $\text{N}-\text{CH}_3$ ), 5.16 (d, 2H,  $\text{NCH}_2$ ,  $J$  = 3.7 Hz), 5.23 (t, 1H, NH,  $J$  = 3.7 Hz), 6.70 (d, 2H,  $J$  = 8.3 Hz), 6.90 (d, 2H,  $J$  = 8.3 Hz), 7.28 (d, 2H,  $J$  = 8.5 Hz), 7.45 (d, 2H,  $J$  = 8.2 Hz), 7.83 (d, 2H,  $J$  = 8.5 Hz), 7.89 (d, 2H,  $J$  = 8.2 Hz); Mass spectrum  $m/z$  106 ( $\text{CH}_2-\text{NH}-\text{C}_6\text{H}_4$ ), 134 ( $\text{N}(\text{CH}_3)-\text{C}_6\text{H}_4-\text{NHCH}_2$ ), 148 ( $\text{C}_6\text{H}_4-\text{N}(\text{CH}_3)\text{COCH}_3$ ), 176 ( $\text{CH}_2-\text{NH}-\text{C}_6\text{H}_4-\text{N}(\text{CH}_3)\text{COCH}_3$ ), 310 ( $\text{CH}_3\text{CON}(\text{CH}_3)-\text{C}_6\text{H}_4-\text{N}=\text{N}-\text{C}_6\text{H}_4-\text{NCOCH}_3$ ), 486 ( $\text{M}^+$ ).

The molar-extinction coefficients of the photo-products at 300 nm were measured by JASCO V-570 UV-vis spectroscopy ( $\epsilon_{300} = 9.3 \times 10^3 \text{ dm}^3 \text{ mol}^{-1} \text{ cm}^{-1}$  for **3d**,  $\epsilon_{300} = 2.0 \times 10^3 \text{ dm}^3 \text{ mol}^{-1} \text{ cm}^{-1}$  for **5**,  $\epsilon_{300} = 4.1 \times 10^3 \text{ dm}^3 \text{ mol}^{-1} \text{ cm}^{-1}$  for **3e**,  $\epsilon_{300} = 1.2 \times 10^3 \text{ dm}^3 \text{ mol}^{-1} \text{ cm}^{-1}$  for **4**). The product ratios of **3d** vs. **5** and **3e** vs. **4** were evaluated by intensities of absorption maxima divided by the molar-extinction coefficient, respectively.

**General Procedure of Quantitative Analysis.** Finely ground powdered crystals of aryl azides (150 mg) were placed in an ESR sample tube, equipped with a hand-made gas-buret. The gas pressure inside the gas-buret was kept at the atmosphere pressure by connecting the outlet to a water stopper through a flexible tube. The ESR sample tube was set in an ESR cavity and UV irradiation was carried out at 203 K for 30 min by an ultrahigh mercury lamp (Ushio USH-500D) through a cut-off filter (Toshiba Glass IRA-25S) to absorb radiative heat. A light beam was focussed on a sample in the cavity through a quartz lens ( $f$  = 100 mm). Liquid nitrogen was used as coolant, and the temperature inside the ESR cavity was

controlled by a JEOL ES-DVT2 temperature controller unit. The amount of evolved nitrogen molecules was measured by reading the change of the gas volume ( $0.707 \text{ cm}^3$  per scale<sup>64</sup>). After UV irradiation, the temperature in the cavity was raised every 20 K and maintained at the temperature. The volume change of the nitrogen gas was measured every ten minutes. The temperature was raised by another 20 K when the volume change stopped.

**General Procedure for Electron Spin Resonance Measurements.** Measurements were carried out with a JEOL JES-RE2X ESR spectrometer & electromagnet, and a JEOL X-band microwave controller. Frequency was measured with an Advantest microwave counter TR5212, and magnetic field with a JEOL ES-FC5 NMR field meter. ESR spectra in the solid state were recorded using ground samples in order to remove any anisotropic effect. Degassing of the 2-methyltetrahydrofuran matrix was performed by freeze-thaw cycles. UV irradiation was carried out by an ultrahigh pressure mercury-lamp (Ushio USH-500D) through a cut-off filter (Toshiba Glass IRA-25S) to absorb radiative heat. A light beam was focussed on a sample tube in the cavity through a quartz lens ( $f = 100 \text{ mm}$ ).

The temperature of a liquid nitrogen cryostat was controlled and measured by a JEOL ES-DVT2 temperature controller unit. Temperature control of a liquid helium cryostat was performed by a Scientific Instruments Inc. 3700 digital temperature indicator/controller, and also with an Advantest Digital multi-thermometer TR2114H with a gold-iron thermocouple.

**General Procedure for X-Ray Crystallographic Analysis.** Single crystals of azides **1a–d** were prepared by recrystallization, while that of **1e** was prepared by sublimation. X-Ray diffraction data of azides **1a–d** were collected at room temperature (Data of **1e** was collected at 203 K) on a Rigaku AFC-5S four-circle diffractometer by using graphite monochromated Mo  $K\alpha$  radiation. Unit cell parameters were determined by least-square refinement of 25

strong reflections. Data were collected with three check reflections monitored after every 100 reflections. Data having  $F < 3\sigma(F)$  were rejected. The structures were solved by direct methods using SAPI85 and refined by a block diagonal least-square refinement.

### Appendix I.

The zfs parameters of the quintet signal derived from a loosely coupled pair of triplet species can be calculated by the following equation. They reflect the relative orientation of the main axes of the two triplet units.<sup>62</sup> Itoh described the entire procedure, taking loosely coupled dicarbene as an example. A dipolar interaction tensor ( $D_Q$ ) of a quintet dicarbene can be expressed by a sum of dipolar tensors ( $D_{T1}$ ,  $D_{T2}$ ) of the individual triplet carbene units under the conditions of weak interaction, where the dipolar tensors are described in the same coordinate system. This procedure can also be applied to loosely coupled arylnitrenes. The principal values of its  $D$  tensor were calculated from the zfs parameters of nitrene **2a** determined by an ESR measurement in a 2-methyltetrahydrofuran glass at 4 K.

$$D_T = (-1/2)(D_{T1} + D_{T2}), \quad D_Q = (1/6)(D_{T1} + D_{T2}).$$

### Appendix II.

Relative energy levels of the spin states in two weakly interacting triplet nitrene species were calculated as follows.<sup>62</sup> The energy of the quintet state ( $S_T=2$ ) is  $-2J$ , and those of the triplet ( $S_T=1$ ) and the singlet state ( $S_T=0$ ) are  $2J$  and  $4J$ , respectively, where  $S_T$  is the total spin quantum number. The energy levels of an antiferromagnetically interacting pair with a negative  $J$  value is shown in Fig. 17a. Since the energy difference ( $\Delta E$ ) between the spin states has a relation of  $\Delta E_{QT} = 2\Delta E_{TS}$ , the temperature dependence of the signal intensities in the ESR spectrum ( $I_S$ ,  $I_T$ ,

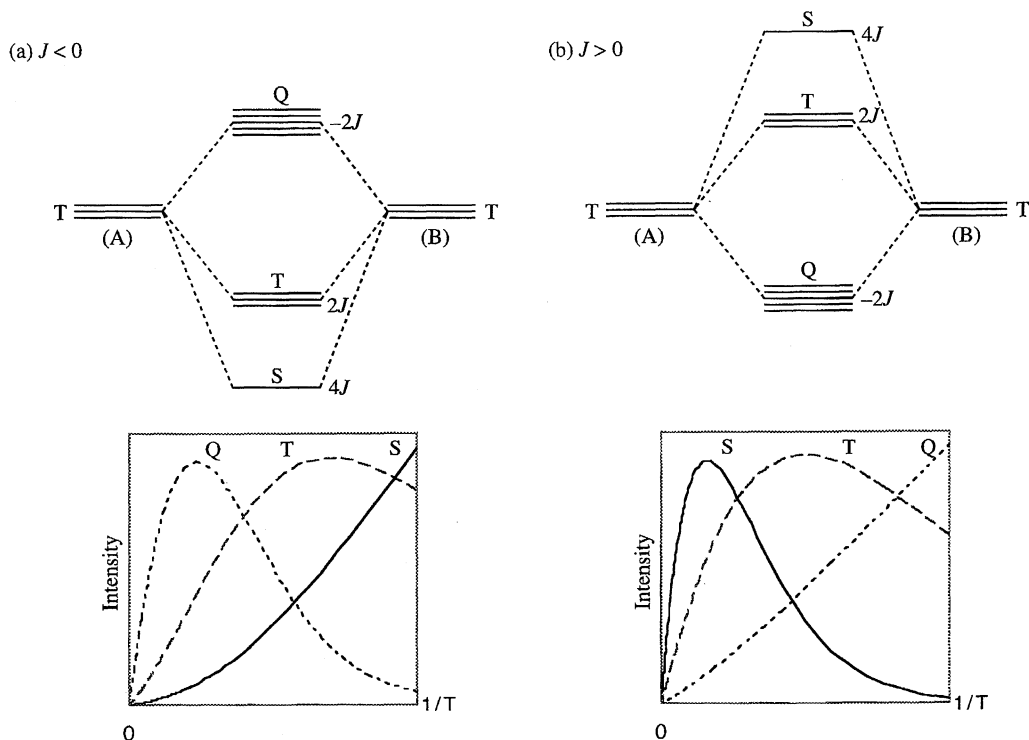


Fig. 17. Weak-interaction diagrams between two triplet nitrenes A and B, and temperature dependence of the ESR signal intensities of singlet (S), triplet (T), and quintet (Q) species. Antiferro- and ferromagnetic interactions are shown in (a) and (b), respectively.

$I_Q$ ) can be expressed by Eqs. 4, 5, and 6, assuming a Boltzmann distribution among the three states, as follows:

$N$  is the number of all the radicals and  $N_S$ ,  $N_T$ , and  $N_Q$  indicate the occupied numbers of radicals in the ground singlet state, thermal triplet, and quintet states, respectively.

$$N = N_S + N_T + N_Q \quad (1)$$

$N_S$ ,  $N_T$ , and  $N_Q$  are assumed to follow the Boltzmann distribution:

$$N_T/N_S = 3 \exp(-2J/kT), \quad (2)$$

$$N_Q/N_S = 5 \exp(-6J/kT), \quad (3)$$

where  $k$  is the Boltzmann constant. Then  $I_S$ ,  $I_T$ , and  $I_Q$  are calculated from Eqs. 1, 2, and 3 (See the graph shown in Fig. 17a),

$$I_S = CN / \{1 + 3 \exp(-2J/kT) + 5 \exp(-6J/kT)\} \cdot T, \quad (4)$$

$$I_T = 3CN \exp(-2J/kT) / \{1 + 3 \exp(-2J/kT) + 5 \exp(-6J/kT)\} \cdot T, \quad (5)$$

$$I_Q = 5CN \exp(-6J/kT) / \{1 + 3 \exp(-2J/kT) + 5 \exp(-6J/kT)\} \cdot T, \quad (6)$$

where  $C$  means a constant. Based on the temperature dependence of the triplet and the quintet signal intensity,  $J$  between a pair of nitrenes **2g** was estimated to be  $-79 \text{ J mol}^{-1}$  according to the above calculation (Fig. 11).

When  $J$  is a positive value,  $I_S$ ,  $I_T$ , and  $I_Q$  are calculated by the same procedure as above (Fig. 17b):

$$I_S = CN \exp(-6J/kT) / \{5 + 3 \exp(-2J/kT) + \exp(-6J/kT)\} \cdot T, \quad (7)$$

$$I_T = 3CN \exp(-2J/kT) / \{5 + 3 \exp(-2J/kT) + \exp(-6J/kT)\} \cdot T, \quad (8)$$

$$I_Q = 5CN / \{5 + 3 \exp(-2J/kT) + \exp(-6J/kT)\} \cdot T. \quad (9)$$

This work was partially supported by a Grant-in-Aid for Scientific Research on Priority Areas No. 06242102 from Ministry of Education, Science, Sports and Culture. This work has been also supported by the CREST (Core Research for Evolutional Science and Technology) of the Japan Science and Technology Corporation (JST).

## References

- 1) A. Gavezzotti and M. Simonetta, *Chem. Rev.*, **82**, 1 (1982).
- 2) J. J. Titman, Z. Luz, and H. W. Spiess, *J. Am. Chem. Soc.*, **114**, 3765 (1992).
- 3) K. Müller, H. Zimmermann, C. Krieger, R. Poupko, and Z. Luz, *J. Am. Chem. Soc.*, **118**, 8006 (1996).
- 4) G. M. J. Schmidt, *Pure Appl. Chem.*, **27**, 647 (1971).
- 5) M. D. Cohen and B. S. Green, *Chem. Br.*, **9**, 490 (1973).
- 6) G. N. Patel, R. R. Chance, E. A. Turi, and Y. P. Khanna, *J. Am. Chem. Soc.*, **100**, 6644 (1978).
- 7) A. D. Gudmundsdottir, T. J. Lewis, L. H. Randall, J. R. Scheffer, S. J. Rettig, J. Trotter, and C. Wu, *J. Am. Chem. Soc.*, **118**, 6167 (1996).
- 8) A. G. Schultz, A. G. Taceras, R. E. Taylor, F. S. Tham, R. K. Kullnig, G. N. Patel, R. R. Chance, E. A. Turi, and Y. P. Khanna, *J. Am. Chem. Soc.*, **114**, 8725 (1992).
- 9) F. Toda and K. Akagi, *J. Org. Chem.*, **55**, 3446 (1990).
- 10) K. Tanaka, S. Kishigami, and F. Toda, *J. Org. Chem.*, **56**, 4333 (1991).
- 11) F. Toda, H. Miyamoto, and S. Kikuchi, *J. Chem. Soc., Chem. Commun.*, **1995**, 621.
- 12) F. Toda, *Acc. Chem. Res.*, **28**, 480 (1995).
- 13) R. R. Chance and G. N. Patel, *J. Polym. Sci., Polym. Phys. Ed.*, **16**, 859 (1978).
- 14) S. H. Shin, A. E. Keating, and M. A. Garcia-Garibay, *J. Am. Chem. Soc.*, **118**, 7626 (1996).
- 15) S. H. Shin, D. Cizmeciyan, A. E. Keating, S. I. Khan, and M. A. Garcia-Garibay, *J. Am. Chem. Soc.*, **119**, 1859 (1997).
- 16) A. J. Arduengo, III, R. L. Harlow, and M. Kline, *J. Am. Chem. Soc.*, **113**, 361 (1991).
- 17) H. Tomioka, J. Nakajima, H. Mizuno, T. Sone, and K. Hirai, *J. Am. Chem. Soc.*, **117**, 11355 (1995).
- 18) H. Tomioka, T. Watanabe, K. Hirai, K. Furukawa, T. Takui, and K. Itoh, *J. Am. Chem. Soc.*, **117**, 6376 (1995).
- 19) B. Iddon, O. Meth-Cohn, E. F. V. Scriven, H. Susehitzky, and P. T. Gallagher, *Angew. Chem., Int. Ed. Engl.*, **18**, 900 (1979).
- 20) E. Leyva and M. S. Platz, *Tetrahedron Lett.*, **26**, 2147 (1985).
- 21) G. Terrones and A. J. Pearlstein, *J. Am. Chem. Soc.*, **113**, 2132 (1991).
- 22) R. N. McDonald and S. J. Davidson, *J. Am. Chem. Soc.*, **115**, 10857 (1993).
- 23) N. P. Gritsan, H. B. Zhai, T. Yuzawa, D. Karweik, J. Brooke, and M. S. Platz, *J. Phys. Chem. A*, **101**, 2833 (1997).
- 24) D. A. Hrovat, E. E. Waali, and W. T. Borden, *J. Am. Chem. Soc.*, **114**, 8698 (1992).
- 25) W. L. Karney and W. T. Borden, *J. Am. Chem. Soc.*, **119**, 3347 (1997).
- 26) T. Ishida, H. Abe, A. Nakajima, and K. Kaya, *Chem. Phys. Lett.*, **170**, 425 (1990).
- 27) B. A. DeGraff, D. W. Gillespie, and R. J. Sundberg, *J. Am. Chem. Soc.*, **95**, 4096 (1973).
- 28) A. K. Schrock and G. B. Schuster, *J. Am. Chem. Soc.*, **106**, 5228 (1984).
- 29) M. S. Platz, *Acc. Chem. Res.*, **28**, 487 (1995).
- 30) O. L. Chapman and J. L. Roux, *J. Am. Chem. Soc.*, **100**, 282 (1978).
- 31) O. L. Chapman, *Pure Appl. Chem.*, **51**, 331 (1979).
- 32) E. Leyva, M. S. Platz, G. Persy, and J. Wirz, *J. Am. Chem. Soc.*, **108**, 3783 (1986).
- 33) A. S. Bailey and J. J. Wedgwood, *J. Chem. Soc. C*, **1968**, 682.
- 34) H. Bock and R. Dammel, *Angew. Chem., Int. Ed. Engl.*, **26**, 504 (1987).
- 35) C. J. Brown and D. E. C. Corbridge, *Acta Crystallogr.*, **7**, 711 (1954).
- 36) A. Sekine and Y. Ohashi, *Acta Crystallogr., Sect. C*, **C50**, 1101 (1994).
- 37) A. Sasaki, A. Izuoka, and T. Sugawara, *Mol. Cryst. Liq. Cryst.*, **277**, 17 (1996).
- 38) L. Mahé, A. Izuoka, and T. Sugawara, *J. Am. Chem. Soc.*, **114**, 7904 (1992).
- 39) R. J. Sundberg, M. Brenner, S. R. Suter, and B. P. Das, *Tetrahedron Lett.*, **1970**, 2715.
- 40) R. J. Sundberg and R. W. Heintzelman, *J. Org. Chem.*, **39**, 2546 (1974).



- 41) J. S. Swenton, T. J. Ikeler, and B. H. Williams, *J. Am. Chem. Soc.*, **92**, 3103 (1970).
- 42) P. A. Lehmen and R. S. Berry, *J. Am. Chem. Soc.*, **95**, 8614 (1973).
- 43) Incidentally, the diradical **N** was found to isomerize to another triplet diradical with zfs parameters of  $|D|=0.0176\text{ cm}^{-1}$ ,  $|E|=0.0014\text{ cm}^{-1}$  at higher temperatures than 150 K.
- 44) K. Ohta, E. R. Davidson, and K. Morokuma, *J. Am. Chem. Soc.*, **107**, 3466 (1985).
- 45) T. Fueno and O. Kajimoto, *J. Am. Chem. Soc.*, **106**, 4061 (1984).
- 46) R. N. McDonald and A. K. Chowdhury, *J. Am. Chem. Soc.*, **102**, 5119 (1980).
- 47) W. H. Waddell and C. L. Go, *J. Am. Chem. Soc.*, **104**, 5804 (1982).
- 48) W. H. Waddell and N. B. Feilchenfeld, *J. Am. Chem. Soc.*, **105**, 5499 (1983).
- 49) E. Leyva, D. Munoz, and M. S. Platz, *J. Org. Chem.*, **54**, 5938 (1989).
- 50) R. Poe, J. Grayzar, M. Jennifer, T. Young, E. Leyva, K. A. Schnapp, and M. S. Platz, *J. Am. Chem. Soc.*, **113**, 3209 (1991).
- 51) R. Poe, K. Schnapp, M. J. T. Young, J. Grayzar, and M. S. Platz, *J. Am. Chem. Soc.*, **114**, 5054 (1992).
- 52) E. Wasserman, G. Smolinsky, and W. A. Yager, *J. Am. Chem. Soc.*, **86**, 3166 (1964).
- 53) J. H. Hall, J. M. Fargher, and M. R. Gisler, *J. Am. Chem. Soc.*, **100**, 2029 (1978).
- 54) S. Sasaki and H. Iwamura, *Chem. Lett.*, **1992**, 1759.
- 55) T. Matsumoto, T. Ishida, N. Koga, and H. Iwamura, *J. Am. Chem. Soc.*, **114**, 9952 (1992).
- 56) A. Izuoka, S. Murata, T. Sugawara, and H. Iwamura, *J. Am. Chem. Soc.*, **109**, 2631 (1987).
- 57) J. M. McBride, *Acc. Chem. Res.*, **16**, 304 (1983).
- 58) T. Sugawara, H. Tukada, A. Izuoka, S. Murata, and H. Iwamura, *J. Am. Chem. Soc.*, **108**, 4272 (1986).
- 59) B. F. LeBlanc and R. S. Sheridan, *J. Am. Chem. Soc.*, **110**, 7250 (1988).
- 60) O. K. Rice and H. C. Ramsperger, *J. Am. Chem. Soc.*, **50**, 617 (1928).
- 61) L. S. Kassel, *J. Phys. Chem.*, **32**, 1065 (1928).
- 62) K. Itoh, *Pure Appl. Chem.*, **50**, 1251 (1978).
- 63) H. Gilman, *Org. Synth.*, Coll. Vol. V, 341 (1932).
- 64) Nitrogen gas of  $0.707\text{ cm}^3$  is equivalent to  $2.9\times 10^{-6}\text{ mol}$  at ambient temperature and pressure, while 150 mg of the azides are equivalent to ca.  $7\text{--}8\times 10^{-4}\text{ mol}$  at least. Assuming that the conversion of azides in UV photolysis of crystals is 3—5%, the evolved nitrogen gas corresponds to  $2\text{--}4\times 10^{-5}\text{ mol}$ . Therefore, the accuracy of this buret is enough for the quantitative analyses of the volume change of the evolved nitrogen.
-